“Clickable” albumin binders for modulating the tumor uptake of targeted radiopharmaceuticals

Brandt, F.; Ullrich, M.; Laube, M.; Kopka, K.; Bachmann, M.; Löser, R.; Pietzsch, J.; Pietzsch, H.-J.; van den Hoff, J.; Wodtke, R.;

Originally published:

December 2021

Journal of Medicinal Chemistry 66(2022)1, 710-733

DOI: https://doi.org/10.1021/acs.jmedchem.1c01791

"Clickable" albumin binders for modulating the tumor uptake of targeted radiopharmaceuticals

Journal:	*Journal of Medicinal Chemistry*
Manuscript ID	jm-2021-01791a.R1
Manuscript Type:	Article
Date Submitted by the Author:	n/a
Complete List of Authors:	Brandt, Florian; Helmholtz-Zentrum Dresden-Rossendorf Institut fur Radiopharmazeutische Krebsforschung; Technische Universitat Dresden, Faculty of Chemistry and Food Chemistry Ullrich, Martin; Helmholtz-Zentrum Dresden-Rossendorf Institut fur Radiopharmazeutische Krebsforschung Laube, Markus; Helmholtz-Zentrum Dresden-Rossendorf Institut fur Radiopharmazeutische Krebsforschung Kopka, Klaus; Helmholtz-Zentrum Dresden-Rossendorf Institut fur Radiopharmazeutische Krebsforschung; Technische Universitat Dresden, Faculty of Chemistry and Food Chemistry Bachmann, Michael; Helmholtz-Zentrum Dresden-Rossendorf Institut fur Radiopharmazeutische Krebsforschung; Technische Universität Dresden, Faculty of Medicine Carl Gustav Carus Löser, Reik ; Helmholtz-Zentrum Dresden-Rossendorf Institut fur Radiopharmazeutische Krebsforschung; Technische Universitat Dresden, Faculty of Chemistry and Food Chemistry Pietzsch, Jens; Helmholtz-Zentrum Dresden-Rossendorf Institut fur Radiopharmazeutische Krebsforschung; Technische Universitat Dresden, Faculty of Chemistry and Food Chemistry Pietzsch, Hans-Jurgen; Helmholtz-Zentrum Dresden-Rossendorf Institut fur Radiopharmazeutische Krebsforschung; Technische Universitat Dresden, Faculty of Chemistry and Food Chemistry van den Hoff, Jörg; Helmholtz-Zentrum Dresden-Rossendorf Institut fur Radiopharmazeutische Krebsforschung; Technische Universität Dresden, Department of Nuclear Medicine, University Hospital Carl Gustav Carus Wodtke, Robert; Helmholtz-Zentrum Dresden-Rossendorf Institut fur Radiopharmazeutische Krebsforschung

“Clickable” albumin binders for modulating the tumor uptake of targeted radiopharmaceuticals

Florian Brandt[a,b], Martin Ullrich[a], Markus Laube[a], Klaus Kopka[a,b], Michael Bachmann[a,c], Reik Löser[a,b], Jens Pietzsch[a,b], Hans-Jürgen Pietzsch[a,b], Jörg van den Hoff[a,d], Robert Wodtke[a,*]

[a] Helmholtz-Zentrum Dresden-Rossendorf, Institute of Radiopharmaceutical Cancer Research, Bautzner Landstraße 400, 01328 Dresden, Germany

[b] Technische Universität Dresden, Faculty of Chemistry and Food Chemistry, Mommsenstraße 4, 01069 Dresden, Germany

[c] National Center for Tumor Diseases (NCT) Dresden, University Hospital Carl Gustav Carus, Fetscherstraße 74, Dresden 01307, Germany

[d] Technische Universität Dresden, Department of Nuclear Medicine, University Hospital Carl Gustav Carus, Fetscherstraße 74, Dresden 01307, Germany

Abstract:

The intentional binding of radioligands to albumin gains increasing attention in the context of radiopharmaceutical cancer therapy as it can lead to an enhanced radioactivity uptake into the tumor lesions and thus, to a potentially improved therapeutic outcome. However, the influence of the radioligand's albumin-binding affinity on the time profile of tumor uptake depending on the particular albumin-binding affinity have been only partly addressed so far. Based on the previously identified N^{ε}-4-(4-iodophenyl)butanoyl-lysine scaffold, we designed "clickable" lysine-derived albumin binders (cLABs) and determined their dissociation constants towards albumin by novel assay methods. Structure-activity relationships were derived and selected cLABs were applied for the modification of the somatostatin receptor subtype-2 ligand (Tyr^3)octreotate. These novel conjugates were radiolabeled with copper-64 and subjected to a detailed *in vitro* and *in vivo* radiopharmacological characterization. Overall, the results of this study provide an incentive for further investigations of albumin binders for applications in endoradionuclide therapies.

Introduction

Besides the interaction to its molecular target, the pharmacokinetic properties, i.e. absorption, distribution, metabolism, excretion, and toxicity (ADMET), of a drug are crucial for its successful *in vivo* application. One parameter of drugs that is usually measured in the context of ADME properties is the binding to constituents of the plasma (or blood), also called plasma protein binding (PPB). PPB is a biased pharmacokinetic aspect with a high degree of PPB often seen as an undesired characteristic of a drug. However, based on the 'free drug hypothesis', which states that the unbound (or free) drug concentration (c_u) at the therapeutic target rather than the unbound fraction (f_u) of the drug in the plasma determines the *in vivo* efficacy, the perspective of PPB experienced a change rendering a high PPB not unfavorable *per se*. Accordingly, a drug with a high f_u value underlies a high rate of clearance and thus, c_u can be similar to that of a drug with a low f_u value but lower rate of clearance.[1-4]

Among the proteinaceous constituents of the blood plasma (albumin, globulines and fibrinogen), albumin is the most abundant component with concentrations between 35-55 g/L in humans[5] and somewhat lower values in laboratory rodents (10-30 g/L)[6]. It has a molar mass of around 67,000 g/mol and exhibits an extraordinary long half-life of around 19 days that can explained by a molecular recycling mechanism involving the neonatale Fc receptor (nFcR).[7] Furthermore, albumin is a natural carrier of a variety of endogenous molecules, including fatty acids, metal ions, and bilirubin to facilitate their solubility and transportation and is also able to bind exogenous substances including drugs, such as ibuprofen.[8]

The long blood circulation time and binding capacity of albumin for different compounds led to the idea to specifically design drugs with an albumin binding moiety to modify their pharmacokinetic behavior. Probably the most intriguing examples come from drugs for the treatment of diabetes.[9-12] Furthermore, the concept of intentional binding to albumin has also entered the design of chemotherapeutic drugs[13-15] and more recently targeted radiopharmaceuticals for the treatment of cancer.[16, 17] Regarding the latter application, the binding to albumin aims at increasing the time-integral uptake of radioactivity in (and thus the total radiation dose delivered to) the tumor and at decreasing the uptake in normal organs such as kidneys. This increase in tumor uptake is often attributed to the prolonged blood circulation time of the albumin-bound radioligand and a presumed higher affinity of the radioligand to the actual target protein than to albumin.[16, 18-22] However, the explanation seems to be misleading considering the "free drug hypothesis" mentioned above with the underlying interplay between concentration of unbound radioligand in the blood and clearance rate. Accordingly, the time profile of total radioligand is altered in the blood by albumin binding but the area under the

curve (AUC) for the free fraction of radioligand (not bound to albumin) is unaffected. Consequently, the total tumor uptake, which is proportional to the area under the corresponding time activity curve, need not be affected by binding to albumin, only the time activity curve might be altered. In fact, a true net increase of tumor uptake of radioligands requires additional uptake mechanisms to be operational that lead to uptake and retention of albumin-bound radioligand in the tumor.

Generally, albumin-based drug delivery can harness distinct pathways for albumin accumulation in tumors that ultimately lead to an increased uptake of the drug as both the free drug and the albumin-bound drug can enter the tumor. Regarding the pathways for albumin accumulation, a frequently proposed mechanism is the so-called *enhanced permeability and retention* (EPR) effect which can at least partly be explained by passive accumulation of macromolecules and nanoparticles in the interstitium at tumor sites. An enhanced permeability can be attributed to the chaotic, irregular blood vessels formed during tumor growth, while the enhanced retention is thought to be caused by reduced lymphatic drainage from the tumor.[23-25] Worth of note, the *EPR effect* tends to be more pronounced in preclinical xenograft mouse models than in humans and varies also between different tumor entities.[24, 26] In addition to a potentially increased accumulation in the interstitium of tumors, internalization of albumin into tumor cells via nonspecific endocytotic processes (e.g. macropinocytosis)[27] or receptor-mediated pathways,[8, 28-30] to cover their demand for amino acids, is a matter of discussion.

The present study was designed to investigate the degree and the time profile of tumor uptake by radioligands bearing albumin-binding moieties with different binding affinity to albumin compared to analogues radioligands without such moieties. As basis for this, the first part of the study covers N^{ε}-(4-(4-Iodophenyl)butanoyl)-lysine (Lys(IPB))-derived albumin binders as described originally by Dumelin *et al.*[31], but modified with azide and alkyne bearing residues at the α-amino group. This enables the introduction into targeting molecules with the opposing functionality by copper-catalysed azide-alkyne cycloaddition (CuAAC).[32] A small library of such "**c**lickable" **l**ysine-derived **a**lbumin **b**inders (hereinafter referred to as cLABs) was synthesized and their albumin-binding affinity was characterized by novel assay methods allowing the derivation of structure-activity relationships. Within the second part, selected cLABs were coupled to the somatostatin analog (Tyr^3)octreotate (TATE), an agonist for the somatostatin receptor subtype 2 (SSTR2). SSTR2 is a G-protein coupled receptor that is often overexpressed in neuroendocrine tumors (NETs) and radiolabeled analogs of its endogenous ligand somatostatin are in current use for the nuclear medical imaging and therapy of such tumors.[33, 34] Herein, the TATE-albumin binder conjugates were labeled with the positron emitter copper-64 via the chelator NODAGA. The resulting **[^{64}Cu]Cu-NODAGA-cLAB-TATEs** were

characterized in radiopharmacological studies *in vitro* and also *in vivo* with positron emission tomography (PET). The time profile of tumor uptake of these radiotracers was assessed using a mouse pheochromocytoma (MPC) tumor allograft model, which highly expresses SSTR2. Efforts on SSTR2-targeted radioligands are in line with our ongoing interest in the functional characterization and the improvement of the therapy of metastatic pheochromocytomas and paragangliomas, neuroendocrine-related tumors that arise from catecholamine-producing chromaffin tissue of the adrenal glands or extra-adrenal paraganglia, respectively. These tumors often show high SSTR2 levels.[35-39] Consequently, SSTR2 radioligands such as **[^{68}Ga]Ga**- or **[^{64}Cu]Cu-DOTA-TATE** for PET imaging as well as **[^{90}Y]Y**- or **[^{177}Lu]Lu-DOTA-TATE** for peptide receptor radionuclide therapy are becoming increasingly important as effective theranostic options for metastatic pheochromocytomas and paragangliomas.[40]

Results and Discussion

Part I: Synthesis and characterization of cLABs

Acetyl-Lys(IPB)-OH, a lysine derivative with unsymmetric substitution pattern at the α- and ε-amino groups and a free carboxyl group, served as lead structure for the cLABs in the present study. For a rapid access to such compounds, an automated solid-phase synthetic strategy was developed starting from commercially available Fmoc-Lys(Alloc)-OH or Alloc-Lys(Fmoc)-OH which were anchored onto the 2-chlorotrityl chloride (2-ClTrtCl) resin (Scheme 1). This strategy furnished compounds **(*R*)-1a-d** and **(*S*)-1c/1e** in overall yields of 20-42%. Later, we switched the synthetic strategy from solid-phase to synthesis in solution to improve the yields and to prepare the albumin binders in larger scale for perspective functionalizing of target molecules. To reduce the synthesis steps to a minimum, we firstly chose to start from free lysine, which gave **(*R*)-1e** and **(*R*)-1f** in lower overall yields of 23 and 6%, respectively (Scheme 2). However, for our most favorable synthetic approach, we chose either Boc-Lys-OH (for the series of N^{ε}-IPB derivatives) or Lys(Boc)-OH (for the series of N^{α}-4-N_3Bz derivatives) as starting materials, which allowed for the preparation of the lysine-based albumin binders **(*S*)-1f-o** with free carboxyl group in three steps and good overall yields of 19-52% (Scheme 3). The synthetic strategies were also adapted to the synthesis of Lys-NH_2 (**(*S*)-2a-c**) and Lys-OCH_3 (**(*S*)-3a**) derivatives. For a more detailed discussion on the synthetic approaches to the albumin binders see Discussion S1 within the Supporting Information. Overall, 15 cLABs were synthesized by the different synthetic strategies (complemented by 7 further compounds) which were characterized for their albumin-binding affinity.

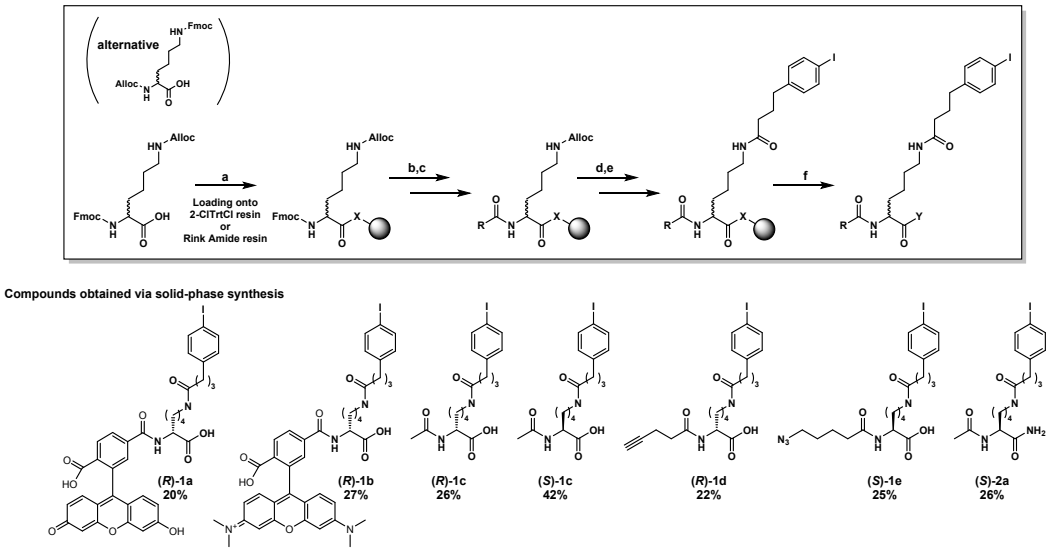

Scheme 1. Solid-phase synthesis of lysine-based albumin binders

Reagents and conditions: $\mathbf{a_1}$) 2-ClTrtCl-resin, DIPEA, CH_2Cl_2, 4 h; $\mathbf{a_2}$) Rink Amide resin, HATU, DIPEA, DMF; **b**) 20% piperidine/DMF; $\mathbf{c_1}$) acetic anhydride, DIPEA, CH_2Cl_2, 2 h; $\mathbf{c_2}$) carboxylic acid derivative, HATU, DIPEA, DMF; **d**) $Pd(PPh_3)_4$, phenylsilane, $CHCl_3$; **e**) 4-(4-iodophenyl)butanoic acid, HATU, DIPEA, DMF; **f**) HFIP/CH_2Cl_2 (1/4), 1 h for 2-ClTrtCl resin and TFA/H_2O/TRIS (95/2.5/2.5), 1 h for Rink amide resin, respectively. With the exception of $\mathbf{a_1}$, $\mathbf{c_1}$ and **f** all reactions were performed in an automated microwave peptide synthesiser. For further details see experimental section. Overall yields are given below the compounds.

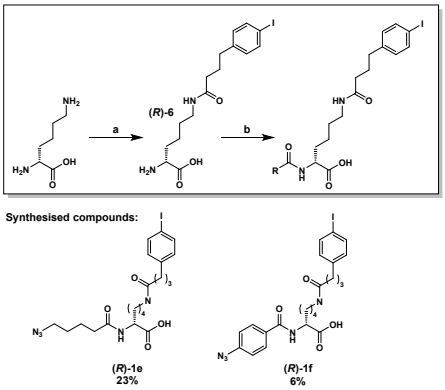

Scheme 2. Synthesis of lysine-based albumin binder in solution starting from fully unprotected lysine

Reagents and conditions: a) 1. $CuSO_4$*$5H_2O$, Na_2CO_3; 2. IPB-NHS (**7a**), H_2O/1,4-dioxane (4/1), 1 d; **b**) 5-azidopentanoic acid NHS ester (**7b**) or 4-azidobenzoic acid (**7c**) NHS ester, TEA, CH_3OH, 20 h. Overall yields are given below the compounds.

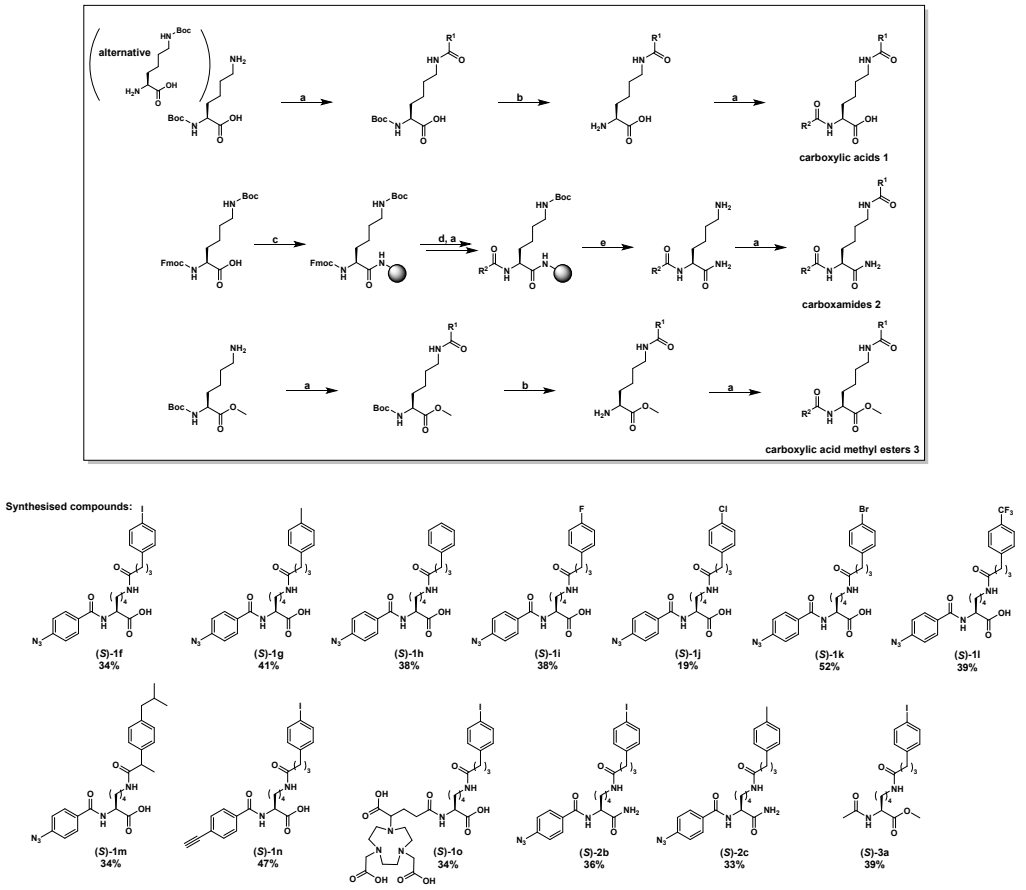

Scheme 3. Optimized synthetic strategy of lysine-based albumin binder

Reagents and conditions: a) Acylations were performed under the following different conditions depending on the carboxylic acids and lysine derivatives: **a_1)** HATU or PyBOP, DIPEA, carboxylic acid, DMF; **a_2)** preactivation of carboxylic acid as NHS (aliphatic carboxylic acids) or HOBt ester (aromatic carboxylic acids) with DIC or DCC, THF/H_2O as solvent mixture; **a_3)** acetic anhydride, DIPEA, CH_2Cl_2; **b)** TFA/CH_2Cl_2 1:1 (v/v), 2 h; **c)** Rink Amide resin, HATU, DIPEA, DMF; **d**) 20% piperidine/DMF; **e)** TFA/H_2O/TRIS (95/2.5/2.5), 1 h; For compound **(*S*)-1o**, the final reaction step was removal of the *tert*-Butyl groups from NODAGA with concentrated H_3PO_4 (see Experimental section). Overall yields are given below the compounds.

To characterize the cLABs by means of their dissociation constants (K_d) towards human serum albumin (HSA), we envisaged a microscale thermophoresis (MST)-based assay. MST represents a rapid method for the characterization of biomolecular interactions in solution that requires only low amounts of sample.[41, 42] Inspired by a recent publication in which MST was used to study the interaction of fluorophore-labeled nanoparticles with HSA[43] and guided by protocols from the company Nanotemper (Explorer Community) for measuring the interactions of bovine serum albumin (BSA) with known ligands, we chose to label commercially available HSA (fatty acid free) using the RED-Maleimide labeling kit (2nd Generation) from Nanotemper. As there is only one free cysteine residue (Cys_{34}) within albumin, this reaction is site-selective, which might prevent a loss of affinity at Sudlow sites I and II.[5] Both sides are the major binding sites for small molecules while binding of the lysine-based albumin binders seems to occur at site II.[31, 44] Indeed, the binding of **(*R*)-1c** (Acetyl-D-Lys(IPB)-OH) and **(*R*)-1f** (N_3Bz-D-Lys(IPB)-

OH) as well as Ibuprofen (site II as primary binding site)[45-47] and Indomethacin (site I as primary binding site)[45] to the fluorophore-labeled HSA led to measurable changes in the thermophoretic timetraces which allowed for the derivation of the respective binding curves (Figure 1A). In this context, we used the freeware PALMIST[48, 49] for data analysis as this program contains different fitting models (see below). While for Ibuprofen (K_d = 73 µM) and Indomethacin (K_d = 120 µM) typical binding curves with one inflection point were obtained (see Figure S1 in Supporting Information), the curves for the lysine-based albumin binders exhibit two inflection points up to concentrations of 2 mM, which indicates binding of two molecules to albumin (Figure 1A for **(*R*)-1f** and Figure S1 for **(*R*)-1c**). Considering that many drugs bind at multiple sites of albumin, this is not surprising. However, it was not known for this class of albumin binders so far. Detection of this phenomenon was only possible as the fluorophore-labeled HSA was titrated with the albumin binders up to high concentrations of 2 mM. For **(*R*)-1c** and **(*R*)-1f** the smaller K_d values were determined to be 8.0 and 2.6 µM, respectively (Table 1), while the higher values lie around 900 µM (1:2 micro fitting model in PALMIST).[48] Dumelin *et al.* determined a lower but still comparable K_d of 3.2 µM for **(*R*)-1c** by isothermal titration calorimetry (ITC).[31] Considering the lower K_d value of **(*R*)-1f** compared to **(*R*)-1c** determined within this study using the same assay method, the benzoyl residue seems to be beneficial for the binding to albumin.

Due to the HSA labeling step, the non-typical binding curves, and the fact that the higher K_d values are less important for the present study, we envisaged a change in the assay settings. Dumelin *et al.* described 5-FAM-D-Lys(IPB)-OH as fluorescent albumin binder and used that probe *i.a.* for a fluorescence anisotropy-based competition assay.[31] We synthesized the respective 6-FAM analogue **(*R*)-1a** in order to establish a MST-based competition assay.[49] However, binding of **(*R*)-1a** resulted in a specific (SDS denaturation test negative, see Figure S2 in Supporting Information) increase in the initial fluorescence signal, which prevents analysis of the MST timetraces. However, a binding curve (Figure 1B) could be derived from the fluorescence values (capillary scans) yielding a K_d value of 230 nM (Table 1), which is in accordance to the K_d value of 310 nM for the 5-FAM analogue determined by ITC.[31] Several mechanisms for the environmental sensitivity of fluorophores are known,[50] however, the particular reason for the increase in fluorescence of **(*R*)-1a** after binding to albumin cannot be given as various aspects including the multiple forms (protolytic and tautomeric) of fluorescein need to be considered.[51] Similarly to the present assay readout, a continuous assay method is known for a long time for transglutaminases which follows an increase in fluorescence due to the enzyme-catalyzed incorporation of mono-dansylcadaverine into e.g. *N*,*N*-dimethylcasein.[52, 53] Worth of note, for the TAMRA derivative **(*R*)-1b**, the increase in

fluorescence after incubation with HSA was unspecific (SDS denaturation test positive, see Figure S2), and thus, this compound was judged not suitable for the assay. Titrating the non-fluorescent albumin binders towards HSA at a constant concentration of **(*R*)-1a** resulted in a dose-dependent decrease of the fluorescence signal (fluorescence-based competition assay) and allowed for the derivation of their K_d values using the 1:1 competition fitting model implemented in PALMIST.[49] For **(*R*)-1c** and **(*R*)-1f**, K_d values of 7.0 and 1.2 µM were obtained, respectively, which are in accordance to the values obtained by the MST assay indicating again the beneficial effect of the benzoyl residue on the affinity to albumin (Table 1).

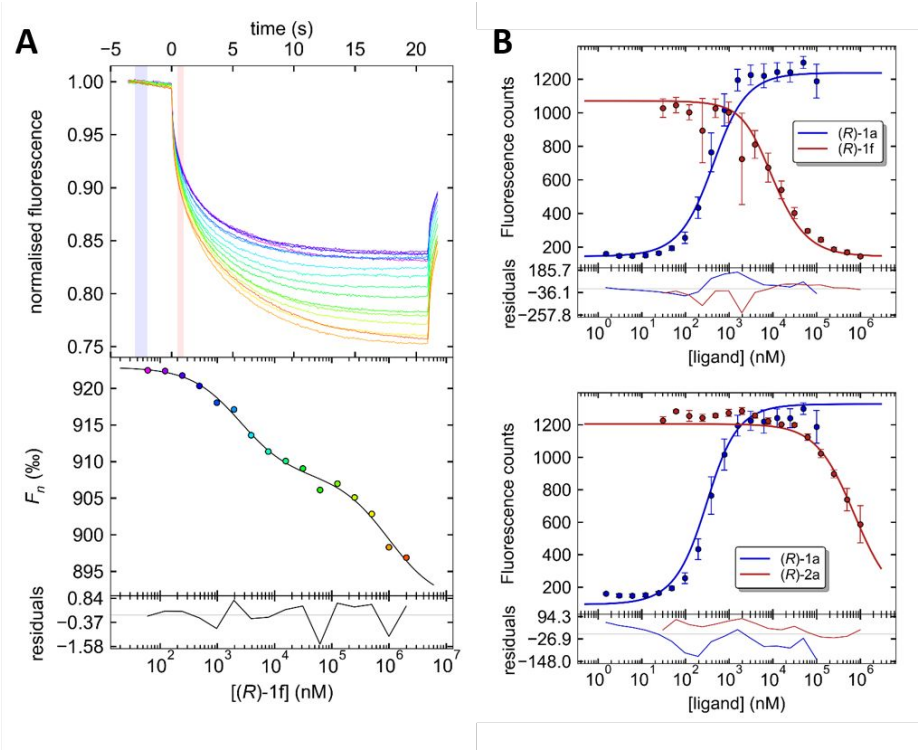

Figure 1. Exemplary data for the MST and fluorescence-based competition assay

A) MST assay: The top panel shows the thermophoretic time traces from one experiment (16 samples, color-coded, purple and orange representing the lowest and highest concentration of **(*R*)-1f**, respectively). The areas used to calculate F_n are shaded in blue and pink (T-jump). The middle panel shows the resulting binding curve (color-coding of data points according to their respective timetrace). The line is the best fit obtained from data analysis using the PALMIST "1:2 Micro" model[48]. Residuals between the fit and the data are depicted in the bottom panel. **B**) Data points for **(*R*)-1a** (blue) are the averaged fluorescence counts (n=6) for the direct titration to HSA. Data points for **(*R*)-1f** (top panel, red) and **(*R*)-2a** (bottom panel, red) are the averaged fluorescence counts (n=3) for the competition experiments. The blue and red lines in each panel represent the results of global fitting of the direct and competition data using the PALMIST "1:1 Comp." model[49]. Residuals are shown below the respective panels. Graphs in A and B were created with GUSSI[54] (version 1.4.2). Conditions for MST assay: PBS pH 7.4, 37°C, 2% DMSO, 100 nM F-HSA, 500 nM HSA; Conditions for fluorescence-based competition assay: PBS pH 7.4, 37°C, 2% DMSO, 2 µM HSA, 200 nM **(*R*)-1a**.

After having established the fluorescence-based competition assay, we screened the further lysine-derived albumin binders by this method (Table 1 and Figure S1 in Supporting Information). Substitution of the acetyl residue in **(*R*)-1c** by a 5-azidopentanoyl residue in **(*R*)-**

1e did not change the binding affinity (7.0 *versus* 8.0). The tolerance for longer alkanoyl residues at the α-amino group was also shown by Dumelin *et al.* as a K_d value of 5.5 µM is stated for Butanoyl-D-Lys(IPB)-OH.[31]

Table 1. Summary of binding affinities for the different lysine-derived albumin binders

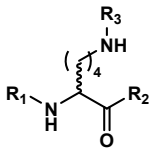

1a-o, 2a-c, 3a

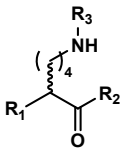

1p

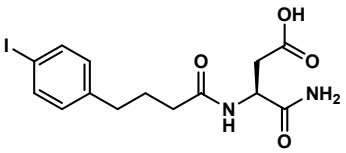

4a

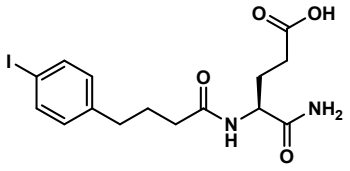

4b

compound	config.	R_1	R_2	R_3	K_d (µM)[a]
1a	*R*	6-FAM	OH	IPB	0.23 (0.17-0.31)[b]
1b	*R*	6-TAMRA	OH	IPB	-[c]
1c	*R*	Acetyl	OH	IPB	7.0 (5.0-11.0)[d]
1c	*S*	Acetyl	OH	IPB	3.2 (1.3-8.9)[e]
1d	*R*	4-Pentynoyl	OH	IPB	7.3 (5.5-9.6)
1e	*R*	5-N_3-Pentanoyl	OH	IPB	8.0 (4.0-14.0)
1e	*S*	5-N_3-Pentanoyl	OH	IPB	6.0 (2.0-12.0)
1f	*R*	4-N_3-Benzoyl	OH	IPB	1.2 (0.6-2.4)[f]
1f	*S*	4-N_3-Benzoyl	OH	IPB	0.36 (0.23-0.56)
1g	*S*	4-N_3-Benzoyl	OH	MPB	3.0 (1.7-5.5)
1h	*S*	4-N_3-Benzoyl	OH	PB	36 (27-50)
1i	*S*	4-N_3-Benzoyl	OH	FPB	26 (17-41)
1j	*S*	4-N_3-Benzoyl	OH	ClPB	3.5 (2.4-5.2)
1k	*S*	4-N_3-Benzoyl	OH	BrPB	2.0 (1.2-3.4)
1l	*S*	4-N_3-Benzoyl	OH	CF_3PB	4.1 (2.9-5.9)
1m	*S*	4-N_3-Benzoyl	OH	IBU	4.0 (2.0-8.0)
1n	*S*	4-Ethinylbenzoyl	OH	IPB	0.34 (0.19-0.60)
1o	*S*	NODAGA	OH	IPB	8.0 (5.0-12.0)
1p	*R*	Phenyltriazol[h]	OH	IPB	4.0 (2.0-8.0)
2a	*S*	Acetyl	NH_2	IPB	70 (50-110)
2b	*S*	4-N_3-Benzoyl	NH_2	IPB	-[g]
2c	*S*	4-N_3-Benzoyl	NH_2	MPB	-[g]
3a	*S*	Acetyl	OCH_3	IPB	110 (60-170)
4a	*S*	-	-	-	100 (60-150)
4b	*S*	-	-	-	80 (50-120)
Ibuprofen	*R/S*	-	-	-	73 (60-90.0)[i]
Indomethacin	-	-	-	-	120 (100-160)[i]

a) K_d data (n≥3, for Indomethacin only n=1) determined by fluorescence-based competition assay if not otherwise stated and are given as mean values with estimated confidence intervals (68.3%) using the error surface projection method in brackets (obtained from PALMIST); b) K_d value determined by titrating **(*R*)-1a** towards HSA; c) no specific binding detected; d) K_d from MST assay is 8.0 (2.0-21.0) µM, K_d from ITC is 3.2 µM[31]; e) K_d from ITC is 9.0 µM[31]; f) K_d from MST assay is 2.6 (0.90-6.8) µM[31]; g) not determined due to low solubility. h) refers to 4-phenyl-1*H*-1,2,3-triazol; i) K_d values obtained from MST assay; Conditions for fluorescence-based competition assay: PBS pH 7.4, 37°C, 2% DMSO, 2 µM HSA (fatty acid free), 200 nM **(*R*)-1a**.

Instead of functionalizing the α-amino group with azide bearing moieties, the incorporation of alkyne bearing substituents appeared also feasible. Compounds **(*R*)-1d** (7.3 µM) and **(*R*)-1n** (0.34 µM) harboring a 4-ethynylbenzoyl and 4-pentynoyl residue, respectively, are equally potent to the analogous azide functionalized albumin binders **(*R*)-1e** and **(*R*)-1f**. Bioisosteric replacement of the α-amide bond to a 1,4-disubstituted 1*H*-1,2,3-triazole[55] was done in **(*R*)-1p**

(Scheme S2 in Supporting Information). Even though the amide bond is preferred, this substitution is well tolerated (4.0 µM of **(*R*)-1p** *versus* 1.2 µM of **(*R*)-1f**).

Dumelin *et al.* demonstrated that the configuration of lysine has only a minor influence on the binding affinity to albumin with a slight tendency to lower K_d values for (*R*)-lysines. To prove this, compounds **(*S*)-1c**/**1e**/**1f** were synthesized, however, we observed an inversed tendency with slightly lower K_d values for the (*S*)-configuration (e.g. 7.0 *versus* 3.2 µM for **(*R*)-** and **(*S*)-1c**, respectively). Therefore, we decided to mainly consider this configuration for our cLABs. We envisaged a series of six 4-N_3Bz-L-Lys(XPB)-OH derivatives which bear differently *para*-substituted 4-phenylbutanoyl residues (X=H, F, Cl, Br, CH_3, CF_3) at the ε-amino group (Table 1). Characterization by the competitive fluorescence-based assay revealed that the unsubstituted derivative (**(*S*)-1h**) exhibits the highest K_d value (36 µM) in this series meaning a 100-fold loss in binding affinity to HSA compared to the iodine substituent (0.36 µM for **(*S*)-1f**). This dramatic loss in binding affinity by simple change of one atom is remarkable and is in accordance to data from Dumelin *et al.*, who determined for 5-FAM-D-Lys(PB)-OH a K_d of 6.6 µM (21-fold loss in binding affinity to the iodine compound with K_d of 310 nM).[31] However, it seems that FAM compensates the iodine/hydrogen exchange better than the 4-azidobenzoyl residue. The binding affinity to HSA for the further derivatives increases in the order F (26 µM) < CF_3 (4.1 µM) < Cl (3.5 µM) < CH_3 (3 µM) < Br (2 µM). The 6-fold and 8-fold loss in binding affinity of the Br and CH_3 derivatives compared to the iodine derivative is also in accordance to data from Dumelin *et al.*, who characterized Acetyl-D-Lys(BrPB)-OH (30 µM, 9-fold loss) and Acetyl-D-Lys(MPB)-OH (52 µM, 16-fold loss) compared to Acetyl-D-Lys(IPB)-OH (3.2 µM).[31]

The trend indicates that the K_d values decrease with the size and the lipophilic character of the substituents. In the context of quantitative structure-activity relationships, the differential van der Waals radii v (Charton values) and Hansch's π values can be used to describe the sterical demand and the lipophilic character of substituents, respectively. As shown in Figure 2, there is a better linear relationship between the π values and the logarithmically transformed K_d values ($R^2 \approx 0.89$) than for the v values ($R^2 \approx 0.65$). However, both correlations can be significantly improved by excluding the data points for the CF_3 derivative (R^2 values of 0.96 and 0.91, respectively) suggesting that a limit in the size of the substituent is reached with v≤0.78 Å (iodine). Worth of note, the use of other substituent parameters such as σ_p and σ_p^- led to significantly worse results for linear regressions (see Figure S3 in Supporting Information). In a recent work towards albumin-binding PSMA ligands, Deberle *et al.* coupled Ibuprofen (IBU) instead of IPB at the side chain of a lysine residue.[56] In order to characterize the effect on the binding affinity to albumin, we synthesized 4-N_3Bz-L-Lys(IBU)-OH (**(*S*)-1m**) using *rac*-2-(4-Isobutylphenyl)propionic acid and determined a K_d value of 4.0 µM which

renders this albumin binder equipotent to the CF_3PB derivative **(*S*)-1l** and 18-fold more potent than simple Ibuprofen (K_d of 73 µM).

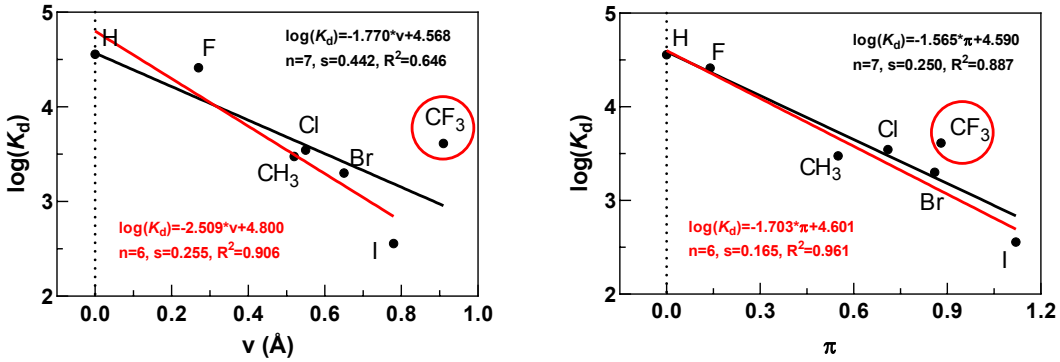

Figure 2. Relationship between the size and the hydrophobicity of the substituents in *para* position of the phenyl residue and the K_d values of the albumin binders (*S*)-1f – (*S*)-1l

Plots of log(K_d)=f(v)(left) and log(K_d)=f(π) (right) using the mean values of the K_d values (nM) of compounds **(*S*)-1f** – **(*S*)-1l** (Table 1) and the following values for v(Å):[57, 58] 0.00 (H), 0.27 (F), 0.52 (CH_3), 0.55 (Cl), 0.65 (Br), 0.78 (I), 0.91 (CF_3); and π:[59] 0.00 (H), 0.14 (F), 0.55 (CH_3), 0.71 (Cl), 0.86 (Br), 0.88 (CF_3), 1.12 (I). Regression analysis was performed by linear regression; n denotes to the amount of data points, s to the standard deviation of the regression equation, and R^2 to the coefficient of determination.[60, 61] For linear regressions in black all data points were considered while for linear regression in red the data for CF_3 were excluded.

In addition to modifications of the residues at the α- and ε-amino groups, we were interested in modifying the free carboxyl group and characterizing the effects on albumin binding. For this, compounds **(*S*)-2a** and **(*S*)-3a** based on Acetyl-L-Lys(IPB)-OH were synthesized in which the carboxyl group is amidated (-NH_2) and esterified (-OCH_3), respectively. These changes led to a dramatic loss in binding affinity (K_d values of 70 and 110 µM meaning factors of 23 and 35), which is however, less pronounced than changing iodine to hydrogen or fluorine (factors of 100 and 72, respectively) as done for the 4-N_3Bz-Lys derivatives. We synthesized also 4-N_3Bz-L-Lys(IPB)-NH_2 (**(*S*)-2b**) and 4-N_3Bz-L-Lys(MPB)-NH_2 (**(*S*)-2c**) for functionalizing the SSTR2 ligands (see below) but were unable to characterize them with the outlined assay methods due to the low solubility of these compounds. However, based on the structure-activity relationships so far, K_d values of around 10 and 60 µM can be predicted (see Discussion S2 in Supporting Information).

In contrast to the original Lys(IPB)-derived albumin binders described by Dumelin *et al.*, Rousseau *et al.* added IPB-Asp or IPB-Glu N-terminally on their somatostatin analogs to simplify the solid-phase synthesis of the peptides.[62] However, they reported no affinity data towards HSA. We synthesized the respective carboxamides **(*S*)-4a** and **(*S*)-4b** (Scheme S3 in

Supporting Information) and determined the K_d values to be 100 and 80 µM, respectively (Table 1), which underlines the importance of the lysine scaffold for the binding affinity to HSA.

Part II: Synthesis and radiopharmacological characterization of the ^{64}Cu-labeled TATE derivatives

On-resin click reaction and radiolabeling

To demonstrate the feasibility of the cLABs, we envisaged a series of four somatostatin receptor subtype 2 (SSTR2) ligands based on the well-known agonist TATE (Figure 3).[63, 64] We denote the novel conjugates as **NODAGA-cLAB-TATEs**. As the introduction of the lysine-derived albumin binders implicate a relatively high structural alteration, we installed a mini PEG2 linker (O2Oc) at the N-terminus to separate the SSTR2 binding motif from the albumin-binding moiety. Propargylglycine was then coupled to the PEG2 linker which was N-terminally acylated with NODAGA, ready for radiolabeling with copper-64. The resulting compound **5** has been synthesized in one sequence using an automated microwave peptide synthesizer (Biotage Initiator+ Alstra). The azide-functionalized albumin binders **(*R*)-1e** and **(*S*)-1f,2b,2c** were chosen for coupling to TATE as they potentially provide peptides with an albumin-binding affinity range of around 1 µM up to 60 µM based on our SAR results and predictions (Table 1 and Discussion S2 in Supporting Information). Coupling was performed by on-resin copper(I)-catalysed azide-alkyne cycloaddition (CuAAC), which ensures undesired complexation of copper by NODAGA due to the protection of the carboxyl groups as *tert*-butyl ester (Scheme S4 in Supporting Information). Subsequent washing with sodium diethyldithiocarbamate in DMF removed adherent copper from the resin. Cleavage from the resin with concomitant removal of all protecting groups was achieved by treatment with TFA in the presence of the scavengers TRIS and water. Cyclization via formation of an intramolecular disulfide bond was realized by dissolving the crude peptide in a mixture of 10% DMSO in CH_3CN/water (25/75) and adjustment of the pH value to pH 8.0.[65, 66] After 48-72 h, the progress of cyclization was usually greater than 90%, which was followed by analytical RP-HPLC. Compound **5** and the four albumin binder conjugates **NODAGA-cLAB(1-4)-TATEs** were obtained in overall yields ranging between 3 and 23% (based on the initial resin loading) and in good chemical purities (>95%, Table 2). For comparison in the subsequent *in vitro* and *in vivo* studies, **NODAGA-TATE** was prepared (Figure 3 and Table 2), while **DOTA-TATE** was commercially available. The identity of all synthesized peptides was also proven by HRMS analysis (Table 2). Labeling of the TATE derivatives with copper-64 by using [^{64}Cu]$CuCl_2$ was performed in an ammonium acetate buffer (final pH value of 4.5) for 20 min at 80°C. This afforded all peptides in good

radiochemical yields and purities (>97%, see Supporting Information for radioactivity-detected chromatograms).

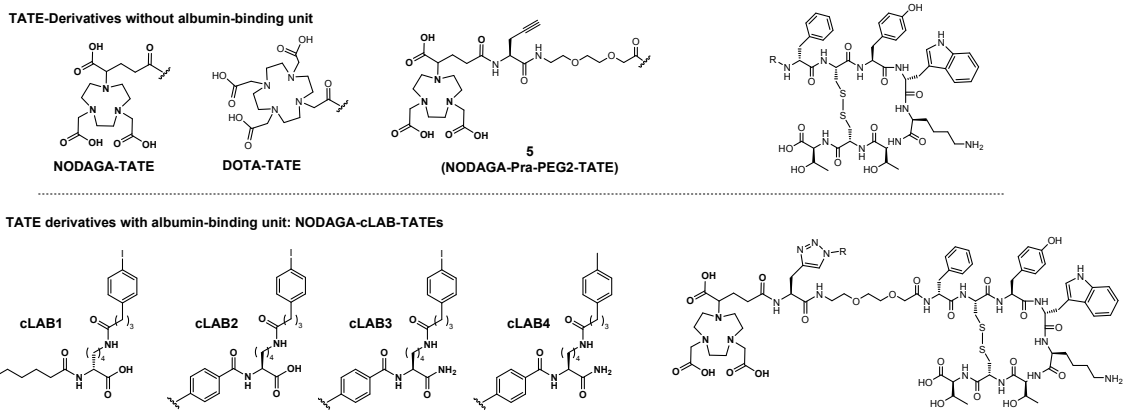

Figure 3. Structures of TATE derivatives used for ^{64}Cu-labeling and subsequent radiopharmacological characterization *in vitro* and in *vivo*

Table 2. Analytical data of the synthesized TATE derivatives

Name	Chemical formula	m/z calculated for $[M+2H]^{2+}$	m/z found for $[M+2H]^{2+}$ [a]	Purity (%)[b]
NODAGA-TATE	$C_{64}H_{87}N_{13}O_{19}S_2$	703.7914	703.7938	≥97.0
5	$C_{75}H_{103}N_{15}O_{23}S_2$	823.8469	823.8475	≥99.0
NODAGA-cLAB1-TATE	$C_{96}H_{133}IN_{20}O_{27}S_2$	1095.4140	1095.4130	≥99.0
NODAGA-cLAB2-TATE	$C_{98}H_{129}IN_{20}O_{27}S_2$	1105.3984	1105.3985	≥97.0
NODAGA-cLAB3-TATE	$C_{98}H_{130}IN_{21}O_{26}S_2$	1104.9064	1104.9071	≥95.0
NODAGA-cLAB4-TATE	$C_{99}H_{133}N_{21}O_{26}S_2$	1048.9659	1048.9680	≥99.0

a) High-resolution mass spectra using electrospray ionization were recorded. b) Purity was determined by analytical RP-HPLC and is given for 230 nm.

Determination of HSA binding and log$D_{7.4}$

To receive a first impression on the effect of the albumin-binding moieties, we performed a radiometric ultrafiltration assay in human plasma, HSA solution and PBS using ultrafiltration devices with a molecular weight limit of 30 kDa (Figure 4A).[18] The ^{64}Cu-labeled peptides without albumin-binding moiety show a remarkable binding to human plasma (46-61%) and only slight binding to HSA (<30% at 3 g/L which corresponds to 45 µM) compared to unspecific binding to the filter membranes in PBS (<20%). In line with these results, non-radioactive **^{175}Lu-DOTA-TATE** is known to be 43%[67] or 50%[68] bound to human plasma proteins, while for **[^{88}Y]Y-DOTA-TATE** a value of 33.4% towards rat plasma proteins is reported.[69] This indicates that the peptides bind either with low affinity to HSA and/or to other components of the blood plasma. In contrast, **[^{64}Cu]Cu-NODAGA-cLAB1-TATE** is almost completely bound to human plasma and HSA (≥95%) under the same conditions, which proves the altered HSA binding properties.

Even though we characterized the isolated albumin binders towards HSA, it is questionable whether this binding affinity is maintained after conjugation to the peptides. To quantify the HSA binding affinity, we advanced the radiometric ultrafiltration assay by keeping the concentration of the radioligand constant (2 µM at 20 GBq/µmol) and varying the concentration of HSA (0.2-2,000 µM). This procedure is analogous to the K_d determination of the fluorescent albumin binder **6-FAM-(*R*)-Lys(IPB)-OH** (**(*R*)-1a**) but inverted to classic radioligand binding experiments. In this context, Müller *et al.* determined K_d values towards HSA for different ^{177}Lu-labeled DOTA-bearing albumin binders by varying the radioligand concentration (spiking with non-radioactive albumin binder) at a fixed HSA concentration.[44] To ensure a true binding regime in our assay, the concentration of the radioligand must be in the range of the expected K_d value (herein 1-50 µM).[70] Initially, we used a molar concentration of 2 µM for the radioligands, which worked well for the peptides without albumin-binding moiety. However, for the four peptides bearing an albumin binder, we noted a very high unspecific binding to the methyl-cellulose membranes in the absence or at low HSA concentrations (up to 70%, Figure 4B). This high unspecific binding has been reduced by using 20 µM of radioligand (at 2 GBq/µmol, data not shown) but the obtained K_d[HSA] value at both radioligand concentrations are similar. Worth of note, commercially available HSA solution in 0.85% sodium chloride should be used instead of HSA solution in 20 mM TRIS/HCl buffer as the use of the latter one resulted in 10-times higher apparent K_d values (data not shown) which might originate from the albumin-binding capability of TRIS itself.[71, 72] Analysis of the resulting binding curves was done by nonlinear regression using the square-root equation I (Morrison equation,[73-75] K_d[HSA] values summarized in Table 3).

$$r = r_{[HSA]=0} + \frac{(r_{[HSA]\to\infty} - r_{[HSA]=0}) * \{([HSA] + [R] + K_d) - \sqrt{([HSA] + [R] + K_d)^2 - 4 * [HSA] * [R]}\}}{2 * [R]} \quad (I)$$

r…percentage of retained radioligand; $r_{[HSA]=0}$…percentage of retained radioligand in the absence of HSA; $r_{[HSA]\to\infty}$…percentage of retained radioligand at infinite concentrations of HSA; [R]…concentration of radioligand

[^{64}Cu]Cu-NODAGA-TATE and **[^{64}Cu]Cu-5** show only weak (unspecific) binding to HSA with estimated K_d values greater than 300 µM. In contrast, the four ^{64}Cu-labeled peptides with albumin-binding moiety exhibit a distinct binding affinity to HSA with K_d values that are largely in accordance to the K_d values of the isolated albumin binders (determined or predicted). The highest binding affinity was observed for **[^{64}Cu]Cu-NODAGA-cLAB2-TATE** (1.8 µM *versus* 0.36 µM of **(*S*)-1f**), followed by **[^{64}Cu]Cu-NODAGA-cLAB1-TATE** (3.1 µM *versus* 8.0 µM of **(*R*)-1e**), **[^{64}Cu]Cu-NODAGA-cLAB3-TATE** (8.5 µM *versus* 10 µM predicted for **(*S*)-2b**) and **[^{64}Cu]Cu-NODAGA-cLAB4-TATE** (53 µM *versus* 60 µM predicted for **(*S*)-2c**). This highlights that the albumin-binding capability of the isolated albumin binders is maintained after

conjugation to the peptides and indicates that a desired albumin-binding affinity can be adjusted for target molecules by choosing from the library of molecules shown in Table 1. Furthermore, the accordance of the calculated and determined K_d values indicate that the contributions to the albumin-binding affinity by the substituents at the different positions are additive.

Table 3. Summary of *in vitro* data for the different ^{64}Cu-labeled TATE derivatives and the albumin binder [^{64}Cu]Cu-(*S*)-1o

compound	$logD_{7.4}$[a]	K_d[HSA] (μM)[b]	K_d[SSTR2] (nM)[c]	B_{max} (fmol/mg of protein)[c]	$t_{1/2}$ (plasma, h)	
					mouse	human
[^{64}Cu]Cu-DOTA-TATE	-3.41 (0.01)	*n.d.*	1.55 (1.38-1.73)	779 (760-798)	>24	*n.d.*
[^{64}Cu]Cu-NODAGA-TATE	-3.43 (0.07)	>300	2.89 (2.51-3.31)	383 (369-397)	>24	*n.d.*
[^{64}Cu]Cu-5	-2.84 (0.09)	>300	4.87 (4.28-5.53)	447 (430-465)	>24	*n.d.*
[^{64}Cu]Cu-NODAGA-cLAB1-TATE	-1.49 (0.08)	3.1	8.57 (6.71-11.0)	1190 (1090-1300)	*n.d.*	*n.d.*
[^{64}Cu]Cu-NODAGA-cLAB2-TATE	-2.25 (0.09)	1.8 (0.1)	6.73 (5.43-8.35)	469 (435-509)	>24	>24
[^{64}Cu]Cu-NODAGA-cLAB3-TATE	-2.12 (0.13)	9.2 (0.9)	2.39 (1.79-3.18)	465 (391-458)	≈6	>24
[^{64}Cu]Cu-NODAGA-cLAB4-TATE	-2.27 (0.16)	50 (2.9)	3.67 (3.30-4.09)	396 (384-408)	≈3	>24
[^{64}Cu]Cu-(*S*)-1o	-3.47 (0.43)	3.0	*n.d.*	*n.d.*	*n.d.*	*n.d.*

Data shown are mean values (±SD or calculated confidence interval of 68%) of a) 3-6 separate processes of shaking out, b) 1-3 single experiments with radioligand concentrations of 2 or 20 μM. c) one experiment which was performed in duplicate. Plasma stability data are obtained in a single experiment. n.d. denotes not determined.

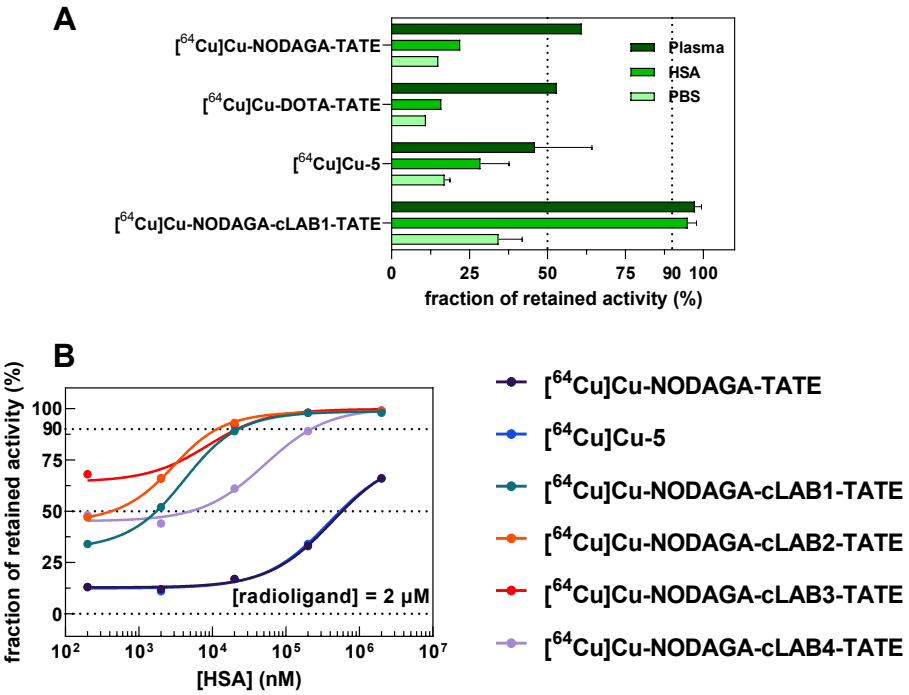

Figure 4. Results of the ultrafiltration assay for the ^{64}Cu-labeled TATE derivatives

A) Data of retained activity for four selected peptides in undiluted human plasma, HSA (3 g/L, in PBS) and PBS (pH 7.4); B) Plots of "fraction of retained activity"=f([HSA]) with nonlinear regressions using equation I (Morrison equation). Data shown are of one single experiment.

To ascertain the influence of the different albumin binders on the physicochemical properties, the $logD_{7.4}$ values of all peptides were determined by the classic shaking flask method (Table 3). **[^{64}Cu]Cu-NODAGA-TATE** and **[^{64}Cu]Cu-DOTA-TATE** served as reference compounds and $logD_{7.4}$ values of -3.43 and -3.41 were determined, respectively, which are in accordance to similar radiometal-labeled derivatives such as **[^{68}Ga]Ga-DOTA-TATE** ($logD_{7.4}$ of -3.69) and **[^{177}Lu]Lu-DOTA-TATE** ($logD_{7.4}$ of -3.16).[76] Compound **[^{64}Cu]Cu-5** equipped with a mini PEG2 linker and propargylglycine between NODAGA and TATE showed a slightly higher $logD_{7.4}$ of -2.84. In contrast, the $logD_{7.4}$ values of the albumin binder functionalized TATE derivatives are around 1.5-2 log units higher substantiating the effect of the lipophilic albumin-binding moiety on the octanol/PBS partition coefficient. Similar results were obtained for other target molecules bearing albumin binders.[77, 78] Worth of note, while **[^{64}Cu]Cu-NODAGA-cLAB2-TATE** and **[^{64}Cu]Cu-NODAGA-cLAB3-TATE** exhibit similar $logD_{7.4}$ values (-2.25 and -2.12, respectively), the respective isolated albumin binders **(*S*)-1f** and **(*S*)-2b** differ significantly in this physicochemical parameter ($logD_{7.4}$ values of 1.75 and 3.13, respectively, as determined by an HPLC method, see Experimental Section). Therefore, the conjugation to the hydrophilic

peptide (including mini PEG2 linker and NODAGA chelator) compensates the actually remarkable difference in the $logD_{7.4}$ between a carboxylic acid and a primary carboxamide.

Characterization of SSTR2 binding

Prior to *in vivo* studies with the novel TATE derivatives, their binding affinity towards SSTR2 was characterized by a radioligand binding assay using cell lysates derived from the mouse pheochromocytoma (MPC) cell line which highly expresses murine SSTR2.[35, 36, 79] K_d and B_{max} data are summarized in Table 3 and saturation binding curves are shown in Figure S5 in Supporting Information. Generally, all novel TATE derivatives are highly potent SSTR2 ligands as their K_d values (2.39-8.57 nM) are comparable to the reference ligands **[^{64}Cu]Cu-NODAGA-TATE** (2.89 nM) and **[^{64}Cu]Cu-DOTA-TATE** (1.55 nM).

In addition to characterize the equilibrium binding to SSTR2 using MPC cell lysates, we were also interested in studying the time-courses of association and dissociation for selected peptides (**[^{64}Cu]Cu-NODAGA-TATE**, **[^{64}Cu]Cu-5** and **[^{64}Cu]Cu-NODAGA-cLAB1-TATE**), which is discussed in detail in Discussion S3 in Supporting Information. In brief, according to a two-step binding model,[80] the introduction of a mini PEG2 linker, propargylglycine and the albumin binders seems to mainly affect the formation of the initial encounter complex between radioligand and receptor by slowing down both the association and dissociation process. This seems to be reasonable as **[^{64}Cu]Cu-5** and **[^{64}Cu]Cu-NODAGA-cLAB1-TATE** exhibit a greater sterical demand than **[^{64}Cu]Cu-NODAGA-TATE**.

Furthermore, an internalization assay was performed with living MPC cells for the peptides **[^{64}Cu]Cu-NODAGA-TATE**, **[^{64}Cu]Cu-5** and **[^{64}Cu]Cu-NODAGA-cLAB1-TATE**. For this purpose, MPC cells were incubated with 2 nM radioligand for 1 h at 4°C and 37°C and total bound radioligand (after washing with PBS pH 7.4) and internalized radioligand (after washing with glycine buffer pH 2.8) were measured (Figure 5).[81] As expected, all compounds show higher values (% dose/mg of protein) of total bound radioligand than internalized radioligand and both processes were significantly reduced at 4°C compared to 37°C (factors of 20-100). **[^{64}Cu]Cu-5** exhibits the lowest values for total binding and also for internalization (12 and 6% dose/mg of protein, respectively). While total binding of **[^{64}Cu]Cu-NODAGA-cLAB1-TATE** (87% dose/mg of protein) is almost twice as high compared to **[^{64}Cu]Cu-NODAGA-TATE** (45% dose/mg of protein), the internalization is comparable (16 and 15% dose/mg of protein, respectively). Therefore, the modification with the albumin-binding moiety seems not to have a detrimental effect on the internalization behavior. Worth of note, internalization of **[^{64}Cu]Cu-NODAGA-TATE** and **[^{64}Cu]Cu-NODAGA-cLAB1-TATE** is also comparable to **[^{64}Cu]Cu-DOTA-TATE** in MPC cells.[36]

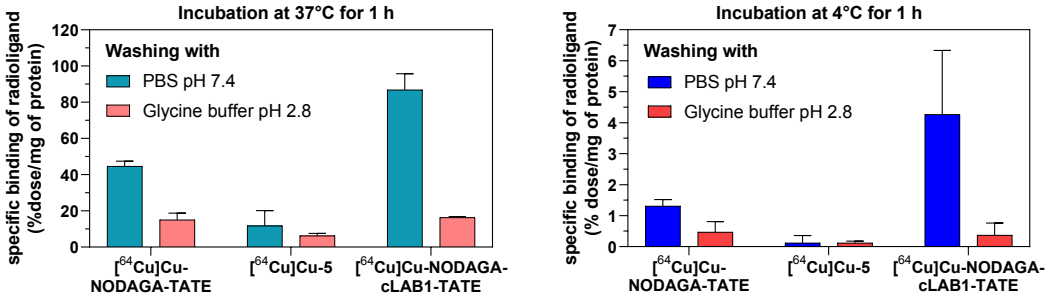

Figure 5. Cell binding data of selected ^{64}Cu-labeled TATE derivatives

Non-specific binding was determined in the presence of 1 µM DOTA-TATE (radioligand concentration of 2 nM). Data shown are mean values (±SD) of one experiment which was performed in triplicate.

Plasma stability

The radiopharmacological characterization of the ^{64}Cu-labeled TATE derivatives was complemented by examination of their stability in mouse and human plasma (Table 3, Figure 6 and Figure S8 in Supporting Information). As expected, **[^{64}Cu]Cu-DOTA-TATE**, **[^{64}Cu]Cu-NODAGA-TATE** and **[^{64}Cu]Cu-5** show excellent stability in mouse plasma ($t_{1/2}$>24 h). A similar stability was observed for **[^{64}Cu]Cu-NODAGA-cLAB2-TATE**. In contrast, **[^{64}Cu]Cu-NODAGA-cLAB3-TATE** and **[^{64}Cu]Cu-NODAGA-cLAB4-TATE** were almost exclusively transformed into one distinct metabolite over 24 h ($t_{1/2}$ of 6 and 3 h, respectively), while stability in human plasma was excellent ($t_{1/2}$>24 h). The common structural characteristics of these two peptides is the primary amide functionality within the albumin-binding moiety. Therefore, we assumed an enzyme-catalyzed hydrolysis of the amide to the respective carboxyl group, which was confirmed by the congruent HPLC retention of the metabolite from **[^{64}Cu]Cu-NODAGA-cLAB3-TATE** with **[^{64}Cu]Cu-NODAGA-cLAB2-TATE** (Figure 6 Left) and by HPLC-DAD-HRMS analysis (Figure S8). Due to the different susceptibility to this transformation in plasma from mouse and human, we supposed that plasma carboxylesterases (Ces) in the mouse plasma are responsible for the degradation of the cLAB3 and cLAB4 derivatives. In this context, the plasma activity of these enzymes is much higher in rodents such as mice and rats while only minor or no activity can be detected in humans.[82-86] To support this assumption, we performed incubations of **[^{64}Cu]Cu-NODAGA-cLAB3-TATE** and **[^{64}Cu]Cu-NODAGA-cLAB4-TATE** in mouse plasma in the presence of BNPP (a specific irreversible inhibitor of carboxylesterases),[85, 87, 88] which largely prevented the degradation of the two peptides (exemplarily shown for the cLAB3 derivative in Figure 6). Although this metabolic transformation does not occur in human plasma, the data suggest using (*R*)-lysine-derived albumin binders (at least for Lys-NH_2 derivatives) in the future, which might not be recognized

by carboxylesterases. The transformation of **[^{64}Cu]Cu-NODAGA-cLAB3-TATE** and **[^{64}Cu]Cu-NODAGA-cLAB4-TATE** to their respective carboxylic acid analogs will be considered for the discussion of the biodistribution data below.

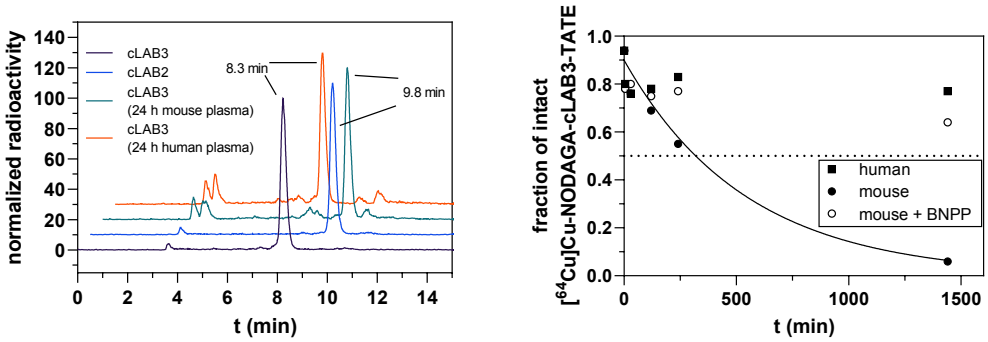

Figure 6. Stability of [^{64}Cu]Cu-NODAGA-cLAB3-TATE in the plasma from mouse and human

Left: radioactivity-detected HPLC chromatograms after ^{64}Cu-labeling and incubations in mouse and human plasma show the transformation of **[^{64}Cu]Cu-NODAGA-cLAB3-TATE** (t_R of 8.3 min) into **[^{64}Cu]Cu-NODAGA-cLAB2-TATE** (t_R of 9.8 min) in mouse plasma but not in human plasma. **Right**: Plot of residual intact **[^{64}Cu]Cu-NODAGA-cLAB3-TATE** under different conditions including nonlinear regression according to one-phase decay for the mouse plasma data (black circles). The dotted line represents a fraction of 0.5. Data shown are obtained in a single experiment. Plasma incubations were performed at 37°C for 24 h and aliquots were withdrawn at distinct time points (5/30 min and 2/4/24 h) for examining the disappearance of the radioligand. For incubation in the presence of BNPP (*bis-para*-nitrophenylphosphate), the mouse plasma had been pre-treated with 300 µM BNPP for 60 min.

Biodistribution of [^{64}Cu]Cu-DOTA-TATE, [^{64}Cu]Cu-NODAGA-TATE and [^{64}Cu]Cu-5

The regional distribution of three ^{64}Cu-labeled SSTR2 ligands without an albumin-binding moiety, **[^{64}Cu]Cu-DOTA-TATE**, **[^{64}Cu]Cu-NODAGA-TATE,** and the alkyne-functionalized derivative **[^{64}Cu]Cu-5**, was evaluated in a subcutaneous MPC tumor allograft model via PET imaging (Figure 7 A-C). All three compounds exhibit substantial SSTR2-specific accumulation in the MPC tumor, followed by partial washout from the tumor site within 48 h. Furthermore, the non-specific accumulation in the liver was low for these three peptides and they were primarily excreted via the renal pathway. The time-*versus*-SUV curves show differences in the kinetic profiles in tumor, heart, and kidneys (Figure 8 A-C; for kinetic profiles in liver and muscle see Figure S8 in Supporting Information), along with the calculated areas under curves ($AUC_{0\text{-}48h}$, Figure 9 A; Table S2 in Supporting Information) and the respective tumor/tissue ratios (Figure 9 B).

For **[^{64}Cu]Cu-DOTA-TATE**, the kinetic profile shows a fast accumulation in the MPC tumor with highest SUVs of around 6.5 after 30 min that were retained up to 2 h followed by washout from the tumor with SUVs of 3.0 and 2.4 after 24 and 48 h, respectively. **[^{64}Cu]Cu-DOTA-**

TATE underlies a rapid clearance from the organism via the kidney, which can be concluded from the sharp SUV maximum of around 14.3 in kidneys shortly after injection and the rapid decline to values <1 after 8 min. In contrast, the maximum SUV was considerably lower in the liver (2.7) but the decline was much slower remaining at rather constant values of around 0.5-1.0 up to 48 h *p.i.* This results in a 2.6-fold higher $AUC_{0\text{-}48h}$ value for the liver (39.0) compared to the kidneys (14.8).

In contrast, **[^{64}Cu]Cu-NODAGA-TATE** showed a reversed liver-to-kidney ratio of the $AUC_{0\text{-}48h}$ values (11.2 for liver and 36.0 for kidneys). Furthermore, the $AUC_{0\text{-}48h}$ of **[^{64}Cu]Cu-NODAGA-TATE** for the blood compartment of the heart was only half the value compared to **[^{64}Cu]Cu-DOTA-TATE** (4.32 *versus* 8.16). A similar trend towards decreased SUVs in liver and heart, but increased SUVs in kidneys has been reported, amongst others, for ^{64}Cu-labeled integrin-targeting RGD peptides conjugated with NODAGA instead of DOTA and has been attributed to higher stability of the copper-NODAGA complex against transchelation of copper in presence of copper-binding proteins compared to copper-DOTA.[89, 90] This potential loss of copper might also explain the lower SUV maximum of **[^{64}Cu]Cu-DOTA-TATE** measured in MPC tumors compared to **[^{64}Cu]Cu-NODAGA-TATE** (6.5 *versus* 9.5). However, the $AUC_{0\text{-}48h}$ values of **[^{64}Cu]Cu-DOTA-TATE** and **[^{64}Cu]Cu-NODAGA-TATE** for the MPC tumors are almost identical (166 *versus* 169). In this context, the lower SUV maximum of **[^{64}Cu]Cu-DOTA-TATE** seems to be compensated by a higher retention in the MPC tumor (SUV_{48h} of 1.4 *versus* 2.4). This could be a result from a higher rate of receptor-mediated endocytosis of [**^{64}Cu]Cu-DOTA-TATE** compared to **[^{64}Cu]Cu-NODAGA-TATE**. Furthermore, uptake of [^{64}Cu]Cu^{2+} released from [**^{64}Cu]Cu-DOTA-TATE** into the tumor by copper transporter proteins could also contribute to the apparent slower washout.[91-93] Further experiments are needed to clarify this.

The third TATE derivative without albumin-binding moiety, [**^{64}Cu]Cu-5**, combines the advantages of low uptake in both kidneys and liver with kinetic profiles similar to those of **[^{64}Cu]Cu-DOTA-TATE** and **[^{64}Cu]Cu-NODAGA-TATE**, respectively. The low liver uptake results clearly from the high stability of the copper-NODAGA complex, however, the low kidney uptake was not expected and indicates a favorable impact of the mini PEG2 linker. The $AUC_{0\text{-}48h}$ value of **[^{64}Cu]Cu-5** in MPC tumors (82.6) was only half the value compared to **[^{64}Cu]Cu-DOTA-TATE** and **[^{64}Cu]Cu-NODAGA-TATE**. However, the tumor-to-kidney $AUC_{0\text{-}48h}$ ratio was still higher for **[^{64}Cu]Cu-5** (7.38) compared to **[^{64}Cu]Cu-NODAGA-TATE** (4.61).

Biodistribution of the different [^{64}Cu]Cu-NODAGA-cLAB-TATEs

In MPC tumor-bearing mice, regional distribution and pharmacokinetic profiles of the four ^{64}Cu-labeled SSTR2 ligands with albumin-binding moiety, **[^{64}Cu]Cu-NODAGA-cLAB(1-4)-TATEs**, differ considerably from the conjugates without albumin binders (Figure 7 D-G and Figure 8 D-G). The radioligands show prolonged blood circulation times resulting in higher SUV_{24h} measured within the blood compartment of the heart (1.6, 2.2, 2.0 and 0.3, respectively) compared to **[^{64}Cu]Cu-NODAGA-TATE** and **[^{64}Cu]Cu-5** (0.08 and 0.03, respectively). Therefore, it is comprehensible that the retention of all four albumin-binding peptides in other well-perfused healthy tissues (kidney, liver, and muscle) is higher compared to the peptides without an albumin-binding moiety (e.g. AUC_{0-48h} values of 58.5 [Kidney], 45.8 [Liver] and 16.6 [Muscle] for **[^{64}Cu]Cu-NODAGA-cLAB2-TATE**).

The AUC_{0-48h} values for the heart correlate with the binding affinity to HSA for the **[^{64}Cu]Cu-NODAGA-cLAB(1-4)-TATEs** and plotting log(AUC_{0-48h}[Heart]) *versus* log(K_d[HSA]) gives a fairly linear relationship (R^2=0.77, Figure 10). Although the binding affinity of the radioligands towards murine serum albumin (MSA) was not determined specifically, it is reasonable to assume a comparable binding behavior based on previous reports.[31] Consequently, due to the increased albumin binding in the blood, accumulation of the **[^{64}Cu]Cu-NODAGA-cLAB(1-4)-TATEs** in MPC tumors was delayed compared to the TATE derivatives without albumin binder resulting in flattened time-*versus*-SUV curves. For example, uptake of **[^{64}Cu]Cu-NODAGA-cLAB2-TATE** with the highest albumin-binding affinity required up to 24 h to reach its maximum SUV of 3.0 in MPC tumors. Plotting log(AUC_{0-48h}[Tumor]) *versus* log(K_d[HSA]) yields a linear relationship (R^2=0.96) meaning the higher the binding affinity to albumin the lower the AUC_{0-48h} values in the MPC tumors for the **^{64}Cu]Cu-NODAGA-cLAB(1-4)-TATEs** (Figure 10). These results indicate that the shifted and flattened tumor uptake curves originate from a reduced initial amount of free radioligand in the blood due to albumin binding, i.e. the better the albumin-binding affinity the lower the free fraction (f_u). Assuming an albumin concentration of 500 µM in the plasma of mice and similar dissociation constants towards MSA, the potential f_u values (and thus, the percentage of albumin-bound radioligand) for the **[^{64}Cu]Cu-NODAGA-cLAB(1-4)-TATEs** in mice can be calculated using the determined K_d[HSA] values (3.1, 1.8, 9.2 and 50 µM, Table 3) and the relation $f_u=K_d[HSA]/(B_{max}+K_d[HSA])$.[94] Accordingly, values of 99.4, 99.6, 98.2 and 91% for albumin-bound radioligand can be derived. The results for the protracted tumor uptake of the **[^{64}Cu]Cu-NODAGA-cLAB(1-4)-TATEs** herein is in line with brain uptake data for *N*-Isopropyl-*p*-[^{123}I]iodoamphetamine, a cerebral perfusion radiotracer, which is strongly bound to serum proteins (75%, mainly to albumin and α_1-acid glycoprotein). Increasing the free fraction of that radiotracer by co-administration of the albumin site II inhibitor

6-methoxy-2-naphthylacetic and/or the α_1-acid glycoprotein site inhibitor erythromycin accelerated the brain uptake significantly.[95] Furthermore, the shift in the time profile of tumor uptake can also be derived from data for the PSMA ligands **^{177}Lu-PSMA-ALB-53** and **^{177}Lu-PSMA-ALB-56** that bear iodine and methyl at the phenylbutanoyl moiety, respectively, and differ 10-fold in their binding affinity to albumin.[96]

In contrast to the tendencies observed for the radioligand kinetics in heart and tumor, all albumin-binding TATEs exhibit a similar shape of the time-*versus*-SUV curves for kidneys (Figure 8 D-G). The corresponding $AUC_{0\text{-}48h}$ values (between 43.5 and 58.8) were significantly higher compared to **[^{64}Cu]Cu-DOTA-TATE** (14.8) and **[^{64}Cu]Cu-5** (11.2), but only slightly higher compared to **[^{64}Cu]Cu-NODAGA-TATE** (36.0). The kinetic profiles for the MPC tumor uptake of all **[^{64}Cu]Cu-NODAGA-cLAB(1-4)-TATEs** exhibit higher $AUC_{0\text{-}48h}$ values than their common precursor peptide **[^{64}Cu]Cu-5** with even higher values for **[^{64}Cu]Cu-NODAGA-cLAB3-TATE** (207) and **[^{64}Cu]Cu-NODAGA-cLAB4-TATE** (289) compared to **[^{64}Cu]Cu-NODAGA-TATE** (166) and **[^{64}Cu]Cu-DOTA-TATE** (169).

As the binding kinetics towards SSTR2 *in vitro* are similar among the TATE derivatives studied herein, other effects might be causative for the enhanced uptake of the albumin binder conjugates in MPC tumors. At first, the higher $logD_{7.4}$ values of the ^{64}Cu-labeled **NODAGA-cLAB-TATEs** point towards an enhanced diffusion coefficient, which in turn might result in increased tissue penetration. Furthermore, additional uptake/retention mechanisms for the albumin-bound radioligand as mentioned in the introduction are likely leading to an additional tumor uptake.[24, 97] To shed light on that particular aspect, we labeled the albumin binder **(*S*)-1o** with copper-64 and compared its *in vivo* distribution with that of the TATE derivatives (Figures 7 H, 8 H and 9). **[^{64}Cu]Cu-(*S*)-1o** has a similar affinity towards HSA (K_d of 3 µM) compared to **[^{64}Cu]Cu-NODAGA-cLAB1-TATE** (Table 3) but shows only low uptake in MPC tumors with highest SUVs of around 1.0 within the initial 2 h after injection along with an $AUC_{0\text{-}48}$ value of 21.0. Furthermore, the $AUC_{0\text{-}48h}$ value for the heart is significantly lower than the respective value for **[^{64}Cu]Cu-NODAGA-cLAB1-TATE** (25.6 *versus* 93.8). In contrast to the TATE conjugates that are mainly excreted via the renal pathway, **[^{64}Cu]Cu-(*S*)-1o** is mainly cleared via the hepatobiliary pathway. At a first glance this appears to be surprising considering the low $logD_{7.4}$ value (-3.43, Table 3) of that compound. The reason for this pharmacokinetic behavior might arise from the fact that this double negatively charged small molecule is potentially a substrate for organic anion transporting polypeptides (OATPs) that mediate the uptake into hepatocytes.[98, 99] Therefore, the tumor uptake of **[^{64}Cu]Cu-(*S*)-1o** might not be representative for the degree of additional tumor uptake observed for the **[^{64}Cu]Cu-NODAGA-cLAB(1-4)-TATEs** compared to TATE derivatives without albumin-binding moiety. However,

the data for **[^{64}Cu]Cu-(*S*)-1o** still indicate that, at least in the MPC tumor model, an additional tumor targeting of the albumin-bound radioligand can be expected to contribute to the total tumor uptake of all **[^{64}Cu]Cu-NODAGA-cLAB(1-4)-TATEs**. Regarding the particular mechanisms, further studies are needed including *ex vivo* autoradiography.[29, 97] An even more representative compound for studying the additional tumor accumulation of the **[^{64}Cu]Cu-NODAGA-cLAB(1-4)-TATEs** herein would be an albumin binder-peptide conjugate with similar physicochemical properties but negligible SSTR2 affinity (e.g. a scrambled sequence of TATE). Such a control experiment has been performed by Chen *et al.* for their truncated Evans Blue/RGD conjugates by using a cyclic pentapeptide with central RAD sequence instead of RGD.[100]

As our plasma stability studies have demonstrated, the primary amide of the albumin-binding moiety in **[^{64}Cu]Cu-NODAGA-cLAB3-TATE** and **[^{64}Cu]Cu-NODAGA-cLAB4-TATE** is hydrolyzed to the carboxyl group in mouse plasma. Consequently, **[^{64}Cu]Cu-NODAGA-cLAB3-TATE** is transformed to **[^{64}Cu]Cu-NODAGA-cLAB2-TATE** ($t_{1/2}$ of around 6 h) accompanied by the respective change to a higher binding affinity to albumin. This might explain the similar kinetic profiles of **[^{64}Cu]Cu-NODAGA-cLAB2-TATE** and **[^{64}Cu]Cu-NODAGA-cLAB3-TATE** measured in heart, kidneys, liver, and muscle and also the fairly linear relationship between the blood retention measured in the heart ($AUC_{0\text{-}48h}$) and the affinity to HSA (Figure 10). In contrast, the uptake of these conjugates in MPC tumors ($AUC_{0\text{-}48h}$) differ considerably (123 *versus* 207, Figure 9 A). This is comprehensible as the lower binding affinity of **[^{64}Cu]Cu-NODAGA-cLAB3-TATE** compared to **[^{64}Cu]Cu-NODAGA-cLAB2-TATE** accounts for an initially higher concentration of unbound radioligand in the blood which facilitates a faster tumor uptake. Therefore, the tumor uptake is barely affected by the metabolic transformation. However, without this transformation the actual $AUC_{0\text{-}48h}$ value of **[^{64}Cu]Cu-NODAGA-cLAB3-TATE** in tumors might be even higher. Similar effects can be expected for **[^{64}Cu]Cu-NODAGA-cLAB4-TATE** even though its carboxylic acid albumin binder analog was not investigated herein.

Among the known albumin-binding SSTR2 ligands,[62, 101] the K_d towards albumin is only reported for a TATE derivative with a truncated Evans Blue moiety as albumin binder (**DOTA-EB-TATE** with K_d[HSA] of 4.8 µM).[19] Thus, the albumin-binding affinity of this peptide lies between **[^{64}Cu]Cu-NODAGA-cLAB1-TATE** (3.1 µM) and **[^{64}Cu]Cu-NODAGA-cLAB3-TATE** (9.2 µM), provided that the affinity of **DOTA-EB-TATE** towards albumin does not depend on the metalation of the chelator moiety in the conjugate. However, e.g. **[^{177}Lu]Lu-DOTA-EB-TATE** achieves a tremendous increase in tumor uptake in a A427-7 xenograft tumor model in mice compared to **[^{177}Lu]Lu-DOTA-TATE** with even higher values at early time points (4 h

p.i.). This is in contrast to the actual protracted accumulation that should result from a distinct binding to albumin (as shown herein). Therefore, we assume that for the EB conjugate an additional or another mechanism exists that contributes to a fast and steadily increasing tumor uptake up to late time points *p.i.*[102] Worth of note, such an elevated tumor uptake for **[^{177}Lu]Lu-DOTA-EB-TATE** has been so far only partly confirmed in first in-human studies.[103, 104]

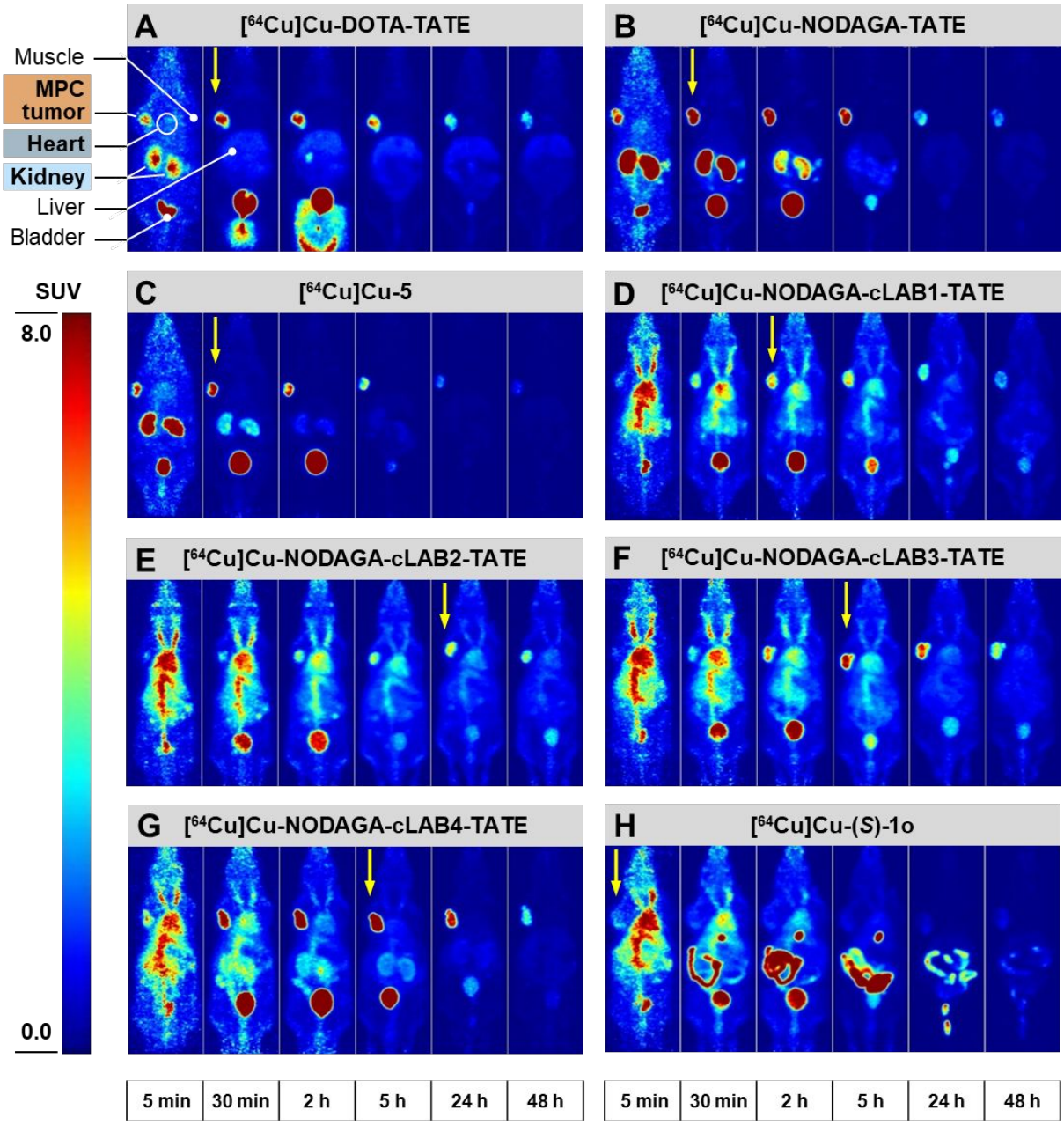

Figure 7. PET images for the different ^{64}Cu-labeled TATEs and the albumin binder [^{64}Cu]-(*S*)-1o

PET images (**A-H**) at selected time points after intravenous injection of the different ^{64}Cu-labeled compounds (7-10 MBq/animal) in MPC tumor bearing mice. Images are presented as maximum intensity projections and shown at common scale. Anatomical positions of tumor, heart, kidney, liver, and muscle, used for SUV quantification are exemplarily shown for **[^{64}Cu]Cu-DOTA-TATE** (**A**). Vertical arrows indicate time points with highest tumor uptake. Indicated time points correspond to the following time frames: 5 min [4-6 min], 30 min [25-40 min], 2 h [105-120 min], 5 h [4.5-5.5 h], 24 h [23-25 h], 48 h [46-50 h].

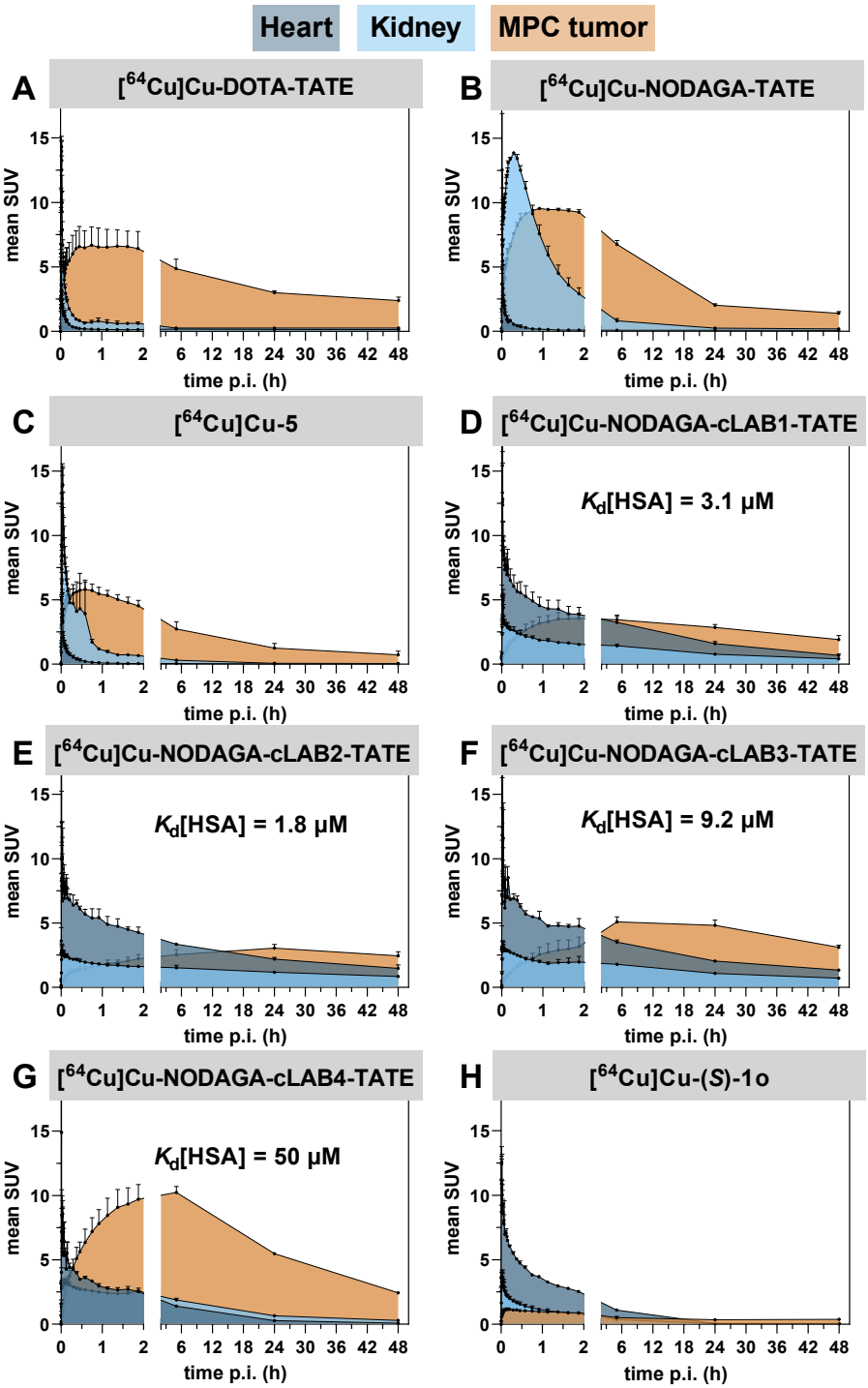

Figure 8. Time-dependent SUV data of heart, kidney and MPC tumor for the different ^{64}Cu-labeled TATE derivatives and the albumin binder (*S*)-1o

In **A-H**, standard uptake values (SUV, decay-corrected) as a function of time (up to 48 h) obtained by PET acquisition (0-2 h in dynamic mode and time points 5, 24 and 48 h p.i.; the x-axes are segmented accordingly) are depicted. Data shown are mean values of a group of MPC tumor-bearing NMRI-nu/nu mice (n=2-3). The area under the respective curves were filled with color for a better visualization (inspired by graphs in Benesova *et al.*[78]).

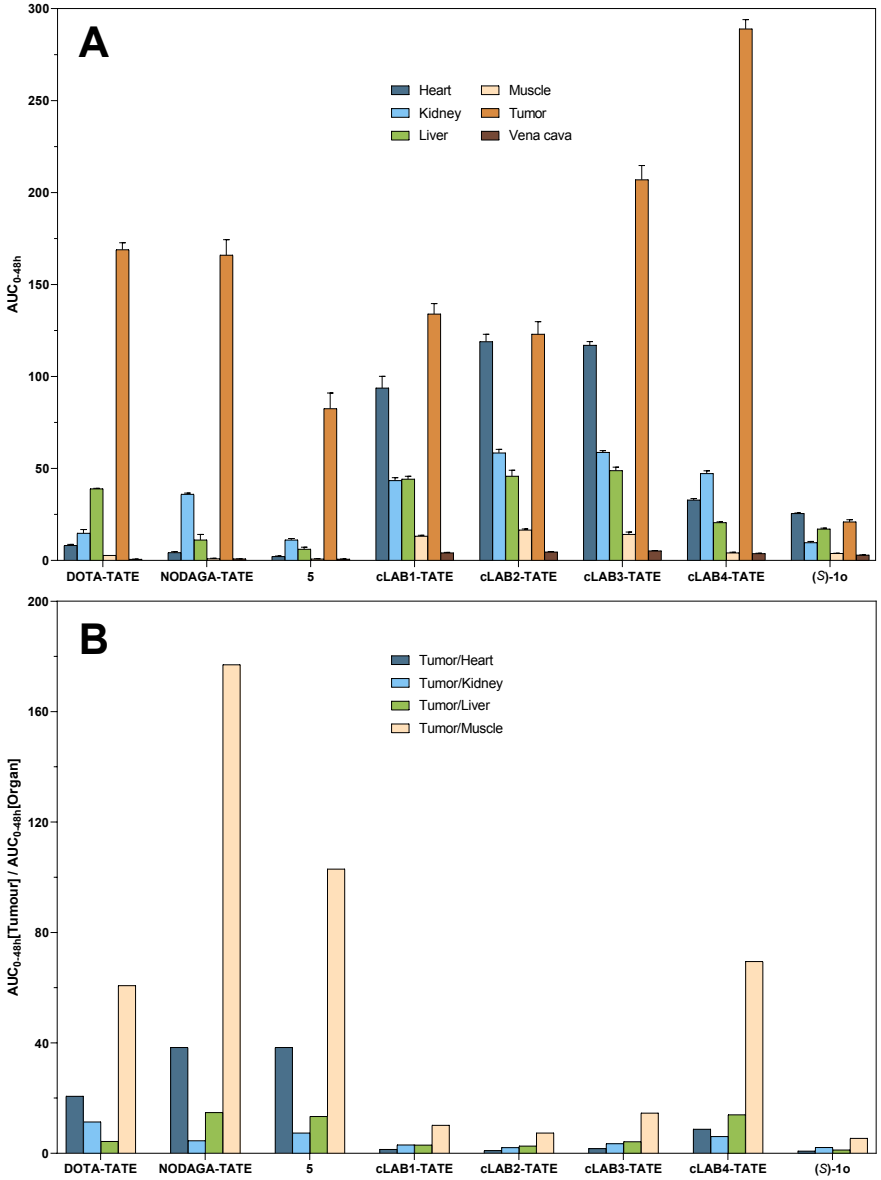

Figure 9. Summary of calculated $AUC_{0\text{-}48h}$ values and the respective Tumor/Organ ratios

Calculated $AUC_{0\text{-}48h}$ values and the Tumor/Organ ratios for the different ^{64}Cu-labeled TATE derivatives and the albumin binder **[^{64}Cu]Cu-(*S*)-1o** are shown in **A** and **B**, respectively. For a better overview, the compound names were abbreviated. The corresponding data table is shown in Table S2 in the Supporting Information. Data shown in **A** are mean values (±SD).

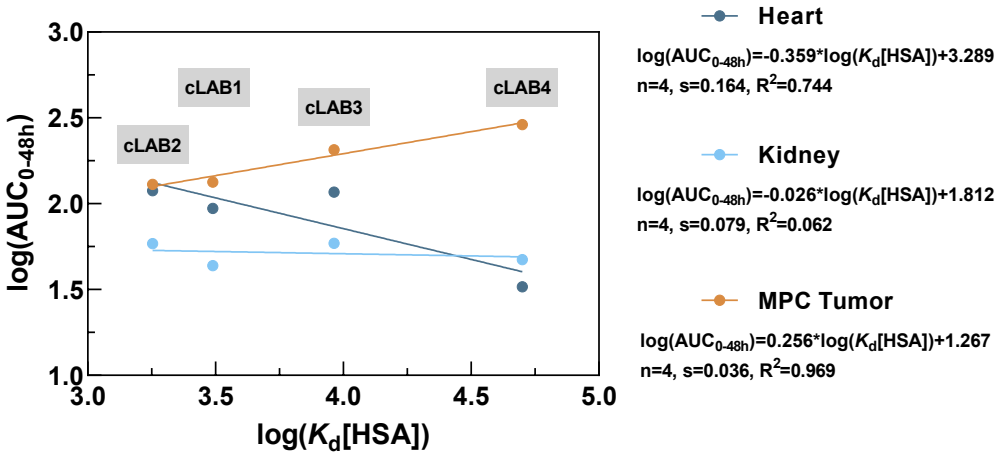

Figure 10. Relationship between $AUC_{0\text{-}48h}$[Organ] and the binding affinity to albumin of the four [^{64}Cu]Cu-NODAGA-cLAB-TATEs

Plots of log($AUC_{0\text{-}48h}$[Organ]=f(log(K_d[HSA])) using the mean values of AUC (Figure 9A and Table S2) and K_d (nM, Table 3) of compounds **[^{64}Cu]Cu-NODAGA-cLAB(1-4)-TATEs**. Regression analysis was performed by linear regression; n denotes to the amount of data points, s to the standard deviation of the regression equation, and R^2 to the coefficient of determination.[60, 61]

Conclusion

The present study demonstrates that the time profile of tumor uptake for ^{64}Cu-labeled SSTR2 ligands is significantly influenced by conjugation to albumin-binding moieties. In particular, the higher the binding affinity of the **[^{64}Cu]Cu-NODAGA-cLAB(1-4)-TATEs** to albumin, the slower is their tumor uptake as the concentration of unbound radioligand is decreased and blood circulation time is increased. Accordingly, the tumor uptake over 48 h increases with lower albumin-binding affinity within the series of **[^{64}Cu]Cu-NODAGA-cLAB(1-4)-TATEs**. Apart from the impact on the time profile, albumin binding leads also to an increase in tumor uptake for the **[^{64}Cu]Cu-NODAGA-cLAB(1-4)-TATEs** compared to analogues radioligands without albumin-binding moieties. In particular, for **[^{64}Cu]Cu-NODAGA-cLAB3-TATE** and **[^{64}Cu]Cu-NODAGA-cLAB4-TATE** the tumor uptake over 48 h significantly exceeds those values of the well-known SSTR2-targeting radioligands **[^{64}Cu]Cu-DOTA-TATE** and **[^{64}Cu]Cu-NODAGA-TATE**. Our data thus suggest an additional tumor retention of the albumin-bound radioligands together with a potentially improved tissue permeation of the radioligands as reasons. Regarding the incorporation of albumin binders into target molecules, the click chemistry approach proved to be a convenient strategy as the albumin-binding affinity of the final radioligand can be predictably modulated based on the used “clickable” lysine-derived albumin binder (cLAB). In future studies, we will extent the **NODAGA-cLAB-TATEs** with derivatives exhibiting an albumin-binding affinity > 50 µM. Furthermore, we will translate the ^{64}Cu-labeled

conjugates to ^{67}Cu- and ^{177}Lu-labeled analogs for further mechanistic studies on the effects of albumin binding.

Experimental Section

General

All commercial reagents and solvents were used without further purification unless otherwise specified. For the incorporation of NODAGA, the building (*R*)-NODA-GA(tBu)$_3$ (CheMatech) was used. DOTA-TATE was purchased from ABX (Radeberg, Germany). Nuclear magnetic resonance spectra were recorded on an Agilent Technologies 400 MR spectrometer consisting of 400/54 premium compact magnet, 400 MR console and 400 MHz OneNMRProbe PT probe head (400 MHz for ^{1}H, 101 MHz for ^{13}C and 376 MHz for ^{19}F) or Agilent Technologies 600 spectrometer consisting of 600/54 premium compact magnet, DD2 console and 600 MHz OneNMRProbe PT probe head (600 MHz for ^{1}H and 151 MHz for ^{13}C). If not stated otherwise, NMR data were obtained at the 400 MR machine. Spectra were processed by using the program MestreNova (version 14.2.1-27684). NMR chemical shifts were referenced to the residual solvent resonances relative to tetramethylsilane (TMS; ^{1}H and ^{13}C) and trichlorofluoromethane ($CFCl_3$; ^{19}F). Mass spectra (ESI) were obtained on a Waters Xevo TQ-S mass spectrometer driven by the Mass Lynx software. All regression analyses were done with GraphPad Prism (version 9.1.2, GraphPad Software, San Diego, CA, USA). The purity of the albumin binders **(*R*)-1a-f**, **(*S*)-1c/e-f**, **(*S*)-2a-c**, and **(*S*)-3a** and the peptides **NODAGA-TATE**, **5**, and **NODAGA-cLAB(1-4)-TATEs** proved to be ≥ 95% as analyzed by a HPLC.

Chromatography

Thin-layer chromatography (TLC) was performed on Merck silica gel F-254 aluminum plates with visualization under UV (254 nm). Preparative column chromatography was carried out on the Flash Chromatography "Selekt System" from Biotage® using appropriate "Sfär" columns and solvent mixtures. The HPLC system used was a LC-20A Prominence HPLC by Shimadzu, consisting of degasser unit DGU-20A5R, two separate pumping units LC-A20R, sample manager SIC-20ACHT, column oven CTO-20AC, PDA-detector SPD-M20A, communication-bus module CBM-20A and fraction collector FRC-10A. Two Aeris Peptide 5 µm XB-C18 columns (100 Å, 250x4.6 mm and 250x21.2 mm) were used as the stationary phases for analytical and preparative RP-HPLC, respectively. A binary gradient system of 0.1% CF_3COOH/water (solvent A) and 0.1% CF_3COOH/CH_3CN (solvent B) at a flow rate of 1 mL/min (analytical) or between 10-20 mL/min (preparative) served as the eluent. High resolution mass spectra (HRMS) were obtained on a Q-TOF MS using electrospray ionization: Agilent 1260 Infinity II HPLC (Santa Clara, California, USA; pump G7111B, autosampler G7129A, column oven G7116N, UV detector G7717C, eluent MeCN/water acidified with 0.1% formic acid 80/20,

bypass mode) coupled to UHD Accurate Mass Q-TOF LC MS G6538A. Unless otherwise stated, the measurements were performed in bypass mode using an eluent consisting of (A): 0.1 % formic acid in CH_3CN and (B): 0.1% formic acid in H_2O; flow rate 0.25 mL/min. Chromatographic separations were performed using a Kinetex XB-C18 column (100A, 2.6 µm, 100x2.1 mm) and the following gradient (A/B): $t_{0\ min}$ 30/70 – $t_{0.5\ min}$ 30/70 – $t_{5.5\ min}$ 60/30 – $t_{6.0\ min}$ 95/5 – $t_{6.5\ min}$ 95/5 – $t_{7.0\ min}$ 30/70 – $t_{12\ min}$ 30/70. A reference mass solution containing ammonium trifluoroacetate, hexakis(1H,1H,3H-tetrafluoropropoxy)phosphazene, and purine was continuously co-injected via dual ESI source. For UPLC-DAD-MS, a system from Waters (ACQUITY UPLC I class system including a ACQUITY UPLC PDA e λ detector coupled to a Xevo TQ-S mass spectrometer) was used. A ACQUITY UPLC BEH C18 column (1.7 µm, 130 Å, 100x2.1 mm, equipped with a ACQUITY UPLC BEH C18 VanGuard Pre-column, 1.7 µm, 130 Å, 5x2.1 mm) was used as stationary phase. A binary gradient system of 0.1% CH_3COOH/water (solvent A) and 0.1% CH_3COOH in CH_3CN/CH_3OH (1:1, v/v, solvent B) at a flow rate of 0.4 mL/min served as the eluent. Analytical radio-HPLC was performed on a Series 1200 device (Agilent Technologies, Santa Clara, CA, USA) equipped with a Ramona ß/γ-ray detector (Raytest, Straubenhardt, Germany). Eluent A: 0.1% (v/v) trifluoroacetic acid in H_2O; eluent B: 0.1% (v/v) trifluoroacetic acid in acetonitrile; HPLC system: Zorbax SB-C18, 300 Å, 4 µm, 250 × 9.4 mm (Agilent); gradient elution using 95% eluent A for 5 minutes, 95% eluent A to 95% eluent B in 10 minutes, 95% eluent B for 5 minutes and 95% eluent B to 95% eluent A in 5 minutes, 3 mL/minute, 50 °C, recovery of activity (decay-corrected) was > 95 %. For the plasma stability measurements of **[^{64}Cu]Cu-NODAGA-cLAB(2-4)-TATEs**, a modified gradient system was used: Gradient elution using 65% eluent A for 5 minutes, 65% eluent A to 85% eluent B in 10 minutes, 85% eluent B for 5 minutes and 85% eluent B to 65% eluent A in 5 minutes, 3 mL/minute, 50°C.

General synthetic procedures

Solid-phase syntheses

With the exception of **GPs I**, **IV**, **VIII** and **IX** all reactions were performed in an automated microwave peptide synthesizer (Initiator+ Alstra from Biotage®).

GP I: General procedure for loading of the 2-ClTrtCl resin with Fmoc-Lys(Alloc)-OH or Alloc-Lys(Fmoc)-OH

For Lys-OH derivatives, 2-ClTrtCl resin (Iris-Biotech, 71 mg, 0.1 mmol, 1.4 mmol/g) was weight into a syringe with frit and suspended in DMF (2 mL) for 30 min. Subsequently, DIPEA (35 µL,

0.2 mmol, 2 eq.) and Fmoc-Lys(Alloc)-OH or Alloc-Lys(Fmoc)-OH (90 mg, 2 eq.) were added. The suspension was shaken for 2 h. After that, the resin was washed with DMF, CH_2Cl_2, CH_3OH and diethyl ether (two times each). The resin was dried under suction for 5 min followed by 30 min at 55°C in an oven. The successful loading was determined by weighing of the resin.

GP II: General procedure for loading of the Rink Amide resin with Alloc-Lys(Fmoc)-OH, Fmoc-Lys(Boc)-OH, Fmoc-Asp(OtBu)-OH or Fmoc-Glu(OtBu)-OH

For Lys-NH_2 derivatives, Rink-amide resin (Fmoc-protected, Biotage, 260 mg, 0.2 mmol, 0.71 mmol/g) was weight into into a syringe with frit and suspended in DMF (2 mL/0.1 mmol) with oscillating mixing and microwave heating (70°C) for 30 min. Fmoc deprotection was done by two cycles of 20% piperidine in DMF (4 mL, 2 mL/0.1 mmol) for 10 min each. The resin was washed with DMF twice and HATU (227 mg, 0.6 mmol, 3 eq., 0.5 M in DMF), DIPEA (210 µL, 0.8 mmol, 6 eq., 2 M in NMP) and Alloc-Lys(Fmoc)-OH (271 mg, 0.6 mmol, 3 eq., 0.2 M in DMF) were added. The coupling was performed with oscillating mixing and microwave heating (75°C) for 5 min. After that the resin was washed with DMF twice.

GP III: General procedure for Fmoc removal

The resin was swollen in DMF (2 mL/0.1 mmol). Fmoc deprotection was done by two cycles of treatment with 20% piperidine in DMF (2 mL/ 0.1 mmol, 10 min each). After that, the resin was washed with DMF twice.

GP IV: General procedure for N^{α}-Acetylation

The resin (0.1 mmol, 0.7 mmol/g) was swollen in DMF (4 mL, 2 mL/0.1 mmol). For acetylation, DMF (4 mL, 2 mL/0.1 mmol), acetic anhydride (95 µL, 1 mmol, 10 eq.) and DIPEA (348 µL, 2 mmol, 20 eq.) were added. The mixture was shaken for 2 h. After that, the resin is washed with DMF and CH_2Cl_2 (two times each).

GP V: General procedure for N^{α}-Acylations (apart from acetylation)

For acylation, the respective carboxylic acid (2 eq., 0.5 M in DMF) was added, followed by HATU (152 mg, 0.4 mmol, 2 eq., 0.5 M in DMF) and DIPEA (138 µL, 0.8 mmol, 4 eq., 2 M in NMP). The coupling was performed with oscillating mixing and microwave heating (75°C) for 5 min. After that the resin was washed with DMF twice.

GP VI: General procedure for N^{ε}-Acylation

For acylation, IPB (166 mg, 0.4 mmol, 2 eq., 0.5 M in DMF) was added, followed by HATU (152 mg, 0.4 mmol, 2 eq., 0.5 M in DMF) and DIPEA (138 µL, 0.8 mmol, 4 eq., 2 M in NMP). The coupling was performed with oscillating mixing and microwave heating (75°C) for 5 min. After that the resin was washed with DMF twice.

GP VII: General procedure for Alloc removal

The resin (0.2 mmol, 0.7 mmol/g) was swollen in CH_2Cl_2 (2 mL/0.1 mmol). The deprotection was done by addition of phenylsilane (370 µL, 3 mmol, 15 eq.) and tetrakis(triphenylphosphine)-palladium(0) (57 mg, 0.05 mmol, 0.25 eq.) in 4 mL $CHCl_3$ (preparation of this solution <30 min before reaction) with oscillating mixing and microwave heating (40°C) for 10 min. After washing with CH_2Cl_2, this cycle was repeated. The resin was washed with sodium diethyldithiocarbamate in DMF (0.5% w/v, 30 mL) and DMF (20 mL).

GP VIIIa: General procedure for the cleavage from the 2-ClTrtCl resin

The resin (0.2 mmol, 0.7 mmol/g) was washed with CH_2Cl_2. 20% HFIP in CH_2Cl_2 was added and shaken for 30 min. The eluate and an additional volume of CH_2Cl_2 (0.5 mL/0.1 mmol) for washing were collected and dried under reduced pressure and N_2 flow. The residue was dissolved in 25% CH_3CN/water and purified by RP-HPLC.

GP VIIIb: General procedure for the cleavage from the Rink amide resin (and concomitant removal of Boc groups)

To the dry resin (0.2 mmol, 0.7 mmol/g) were added TRIS (25 µL/0.1 mmol) and H_2O (25 µL/0.1 mmol) followed by TFA (1 mL/0.1 mmol). The resin was shaken for 30 min. The eluate and an additional volume TFA (0.5 mL/0.1 mmol) for washing were collected and dried under reduced pressure and N_2 flow. The residue was dissolved in 50% CH_3CN/water. In case of a following acylation step, see **GP XIII**, otherwise the solution was purified by RP-HPLC.

GP VIIIc: General procedure for the cleavage of peptides from Wang resin (and concomitant removal of *t*Bu/Boc/Trt groups)

To the dry resin (0.2 mmol, 0.7 mmol/g) were added TRIS (25 µL/0.1 mmol) and H_2O (25 µL/0.1 mmol) followed by TFA (1 mL/0.1 mmol). The resin was shaken for 2 h at 40°C. The eluate and an additional volume TFA (0.5 mL/0.1 mmol) for washing were collected and dried under reduced pressure and N_2 flow. The residue was diluted with 50 mL of diethylether and put in the freezer for at least 3 h before the resulting suspension was centrifugated at 7780 rpm for 10 min. The solution was decanted and 30 ml of cold diethylether was added again. This washing procedure was repeated twice. The final pellet was dried at 55°C for 30 min in an oven.

GP IX: General procedure for on-resin copper-catalysed azide-alkyne cycloaddition (CuAAC)

The peptide resin (0.03 mmol) was swollen in DMF (3 mL/0.1 mmol) for 30 min. After elution of the DMF excess, the azide-functionalized albumin binder (17 mg, 0.03 mmol, 1 eq.) in DMF (2 mL), $CuSO_4*5H_2O$ (4 mg, 15 µmol, 0.5 eq.) and THPTA (7 mg, 15 µmol, 0.5 eq.) in water (245 µL) were added and shaken before addition of sodium ascorbate (29 mg, 0.15 mmol, 5 eq.) in water (105 µL). The suspension was shaken for 2 h. After elution, the resin was washed with DMF (20 mL), sodium diethyldithiocarbamate in DMF (0.5% w/v, 30 mL), DMF (20 mL), CH_2Cl_2 (20 mL), CH_3OH (20 mL) and diethylether (20 mL). The resin was finally dried at 55°C for 30 min in an oven.

Syntheses in solution

GP X: General procedure for N^{ε}-acylation of lysine

D-Lysine*HCl (180 mg, 1 mmol), NaOH (40 mg, 1 mmol, 1 eq.), Na_2CO_3 (100 mg, 1.2 mmol, 1.2 eq.) and $CuSO_4*5H_2O$ (84 mg, 0.55 mmol, 0.55 eq.) were dissolved in water (2 mL) and stirred for 10 min to form a clear, deep-blue solution. IPB-NHS (397 mg, 1.05 mmol, 1.05 eq.) was dissolved in 1,4-dioxane (4 mL) and added in 1 mL steps. The solution was stirred over night. The suspension was filtered through a paper filter and rinsed with 50 mL water. The retained whole filter containing the filter cake was transferred to a 300 mL beaker. The beaker was filled with 250 mL of a 2 mM EDTA solution and heated to 80°C for 1 hour. After cooling, a white solid was formed that was filtered, rinsed with water and finally dried by lyophilization.

GP XI: General procedure for acylations with aliphatic carboxylic acids (preactivated as NHS ester)

To a solution of the carboxylic acid (1 mmol) and NHS (126 mg, 1.1 mmol, 1.1 eq.) in THF (6.5 mL/mmol) was added DCC (226 mg, 1.1 mmol, 1.1 eq.) resulting in the formation of a white precipitate within the first minute. The reaction progress was followed by TLC (CH_2Cl_2:CH_3OH, 98:2, v/v). After 1 h, the suspension was filtered into a solution of Boc-Lys-OH (1.1 eq.) and Na_2CO_3 (3 eq.) in water (5 mL/mmol). The filter cake was rinsed with THF (1.5 mL/mmol). The reaction progress in the eluate was followed by HPLC. After 3 h, the organic solvent was evaporated. The suspension was transferred into a separating funnel and the filter cake was rinsed with water. The pH value was adjusted to 2-3 by the addition of 1 M HCl and the aqueous phase was extracted with ethyl acetate (3×20 mL). The combined organic phases were washed with brine and dried under vacuum overnight. The compounds were purified by column chromatography (CH_3OH/CH_2Cl_2).

GP XII: General procedure for acylations with benzoic acids (preactivated as HOBt ester)

To a solution of the respective benzoic acid (0.2 mmol) and HOBt (30 mg, 0.22 mmol, 1.1 eq.) in THF (6.5 mL/mmol) was added DCC (45 mg, 0.22 mmol, 1.1 eq.) resulting in the formation of white precipitate within the first minute. The reaction progress was followed by TLC (CH_2Cl_2:CH_3OH, 98:2, v/v). After 2 h, the suspension was filtered into a solution of the primary amine (1.0 eq.) and Na_2CO_3 (3 eq.) in water (5 mL/mmol). The filter cake was rinsed with THF (1.5 mL/mmol). The reaction progress was followed by HPLC. After 3 h, the organic solvent was evaporated. The pH value was adjusted to 2-3 by the addition of 1N HCl and the aqueous phase was extracted with ethyl acetate (3×5 mL). The combined organic phases were washed with brine and dried under vacuum overnight. The compounds were purified by column chromatography (CH_3OH/CH_2Cl_2).

GP XIII: General procedure for acylations with carboxylic acid (without preactivation)

The Lys-OMe or Lys-NH_2 derivative (0.2 mmol) was dissolved in 50% CH_3CN in water (2 mL/0.1 mmol), followed by addition of azidobenzoic acid (32 mg, 0.2 mmol, 1 eq.) PyBOP (208 mg, 0.4 mmol, 2 eq.) and Et_3N (111 µL, 0.8 mmol, 4 eq.). After 3 h, the organic solvent was evaporated. The pH value was adjusted to 2-3 by the addition of 1 M HCl and the aqueous phase was extracted with ethyl acetate (3×5 mL). The combined organic phases were washed with brine and dried under vacuum overnight. The compounds were purified by RP-HPLC.

GP XIV: General procedure for Boc removal in solution

The respective Boc-protected compound (0.4 mmol) was dissolved in CH_2Cl_2 (2 mL/mmol) followed by the addition of TFA (2 mL/mmol). The solution was stirred for 2 h. The reaction progress was checked by TLC. After completion, all volatile substances were removed under reduced pressure and N_2 flow. The residue was immediately used for further reactions. In case of storage for a distinct time, water was added to the residue and the mixture was lyophilized.

GP XV: General procedure for TATE cyclization via disulphide formation

The cleaved and dried peptide was weight out. The peptide (50mg, 0.03mmol) was dissolved in CH_3CN/water 1:1 (0.5ml/mg). The pH was adjusted to 8.0 by addition of 1% aqueous ammonia (v/v). The solution was diluted to 25% CH_3CN/water by addition of water. Finally, DMSO was added (10%, v/v final) and stirred for up to 72 h. The progress of cyclization was followed by UPLC-DAD-MS. After completion, the solution was lyophilized and the crude peptide was purified by RP-HPLC.

Assay methods for HSA binding

MST assay

Fatty acid-free human serum albumin (HSA) was labeled using the Monolith Protein Labeling Kit RED-MALEIMIDE 2nd Generation (Cysteine reactive, NanoTemper Technologies). The labeling reaction was performed according to the manufacturer's instructions (Monolith Protocol MO-O-018). In brief, HSA (6.7 µM) was pretreated with TCEP (26.7 µM) in labeling buffer for 30 min at room temperature. Subsequently, the dye was added to obtained the reaction mixture consisting of HSA (5 µM), TCEP (20 µM) and dye (50 µM) in labeling buffer (5% DMSO) and the labeling performed for 30 min at room temperature in the dark. Unreacted dye was removed with the supplied dye removal column equilibrated with PBS (pH 7.4). 500 µL of fluorescently labeled HSA (2 µM) in PBS were obtained.

The labeled HSA (20 µL, 2 µM) was mixed with unlabeled HSA (2 µL, 100 µM in PBS). These mixtures were stored at -80°C. Right before the measurements, PBS (188 µL) was added to achieve a solution with 200 nM labeled HSA and 1 µM unlabeled HSA.

Stock solutions (200 mM) of the albumin binder were prepared in DMSO and were 50-fold diluted with PBS to obtain 4 mM solutions in 2% DMSO. A series of 16 1:1 dilutions were prepared using the same buffer (2% DMSO/PBS), producing ligand concentrations ranging from 122 nM to 4 mM. For the measurement, each ligand dilution was mixed with one volume of the labeled/unlabeled HSA solution (200 / 1000 nM), which led to a final concentration of

labeled/unlabeled HSA of 100 / 500 nM and final ligand concentrations ranging from 61 nM to 2 mM. After 5 min incubation, the samples were loaded into Monolith NT.115 Capillaries (NanoTemper Technologies). MST was measured using a Monolith NT.115 instrument (NanoTemper Technologies) at 37°C operating in Red mode.

Instrument parameters were adjusted to 60% LED power and medium MST power. Data of three independently pipetted measurements were analysed (PALMIST software version 1.4.4) using the signal from an MST-on time of 0.2 s.[48, 49]

Fluorescence-based competition assay

A stock solution (20 µM) of compound **(*R*)-1a** was prepared in DMSO and aliquots thereof were stored at -80°C. HSA was freshly dissolved in PBS to obtain a 100 µM stock solution. Right before the measurements, 4 µL of **(*R*)-1a** (20 µM) and 8 µL of HSA (100 µM) were added to 188 µL of PBS to obtain concentrations of 400 nM and 4 µM, respectivley, in 2% DMSO/PBS.

Stock solutions (100 mM) of the albumin binder were prepared in DMSO and were 50-fold diluted with PBS to obtain 2 mM solutions in 2% DMSO/PBS. A series of 16 1:1 dilutions were prepared using the same buffer (2% DMSO/PBS), producing ligand concentrations ranging from 62 nM to 2 mM. For the measurement, each ligand dilution was mixed with one volume of the **(*R*)-1a**/HSA solution (400 nM / 4 µM), which led to a final concentration for **(*R*)-1a** of 200 nM and for HSA of 2 µM and final ligand concentrations ranging from 31 nM to 1 mM. The further procedure including data processing was similar to the MST assay (see above) with the exception that the initial fluorescence values were used for analysis and the system operated in Green mode.

Determination of $logD_{7.4}$ of (*S*)-1f and (*S*)-2b by HPLC

The $logD_{7.4HPLC}$ value was determined as previously reported by us[105, 106] utilizing a modified HPLC method originally described by Donovan and Pescatore[107]. Hydrocortisone (t_R 10.68 min, log$D_{7.4}$ 1,46 (mean of 1.55[108] and $logD_{7.4}$ 1.37[108]) and triphenylene (t_R 29.67 min, $logD_{7.4}$ 5.49[107]) served as references to calculate $logD_{7.4HPLC}$ as given in formula 4 of reference[107] and toluene (t_R 16.45 min, measured $logD_{7.4HPLC}$ 2.70, Literature $logD_{7.4}$ 2.72[107]) as internal reference. The following HPLC system was used: Agilent 1100 HPLC (binary pump G1312A, autosampler G1313A, column oven G1316A, degasser G1322A, UV detector G1314A, γ detector Gabi Star (Raytest); column ODP-50 4B (Shodex Asahipak 50 x 4.6 mm); eluent: MeOH/ phosphate buffer (10 mM, pH 7.4), gradient $t_{0\ min}$ 30/70 – $t_{25\ min}$ 95/5 – $t_{27\ min}$ 95/5 – $t_{28\ min}$ 30/70 – $t_{40\ min}$ 30/70, flow rate = 0.6 mL/min. Retention times of **(*S*)-1f and (*S*)-2b** were found

to be 12.05 ± 0.01 min and 18.55 ± 0.01 min, which correspond to $logD_{7.4HPLC}$ values of 1.75 and 3.13, respectively.

Radiolabeling of DOTA/NODAGA-bearing peptides

[^{64}Cu]$CuCl_2$ was produced at the Helmholtz-Zentrum Dresden-Rossendorf on the 30 MeV TR-Flex-cylotron (Advanced Cyclotron Systems Inc., ACSI, Canada) by ^{64}Ni(p,n)^{64}Cu nuclear reaction as reported previously.[109, 110]

For a typical radiolabeling procedure, 548 MBq of [^{64}Cu]$CuCl_2$ (60 µL in H_2O) was mixed with 0.01 M HCl (230 µL) and ammonium acetate buffer (2 M, pH 8, 30 µL) to obtain a solution with a pH value around 5.5. An aliquot of this mixture (105 µL) was then added to the peptide stock solution (2.5 µL of 2 mM in 10% DMSO/PBS pH 7.4) and the mixture was incubated for 20 min at 80°C. Quality control of the radiolabeled peptide conjugates was performed by radio-HPLC analysis. Labeling yields were usually ≥97%. The radiolabeled peptides were used without purification. Molar activities of up to 50 GBq/µmol were achieved and were calculated based on the applied peptide amount. For further cell experiments and in vivo application, the reaction mixture was diluted with cell culture medium, phosphate buffered saline (PBS, pH 7.4) or 0.154 mol/L NaCl.

Ultrafiltration assay

An ultrafiltration assay was used to determine the binding of the ^{64}Cu-labeled compounds to plasma proteins and HSA. Centrifree ultrafiltration devices (4104 centrifugal filter units by Millipore; 30,000 Da nominal molecular weight limit, methylcellulose micropartition membranes) were used to separate the free fraction of the radioligand from the protein–bound fraction.[18, 96] The radioligands (0.7 nmol, 12 MBq) in a volume of 25 µL were added to 250 µL of plasma, HSA solutions (3.5 g/L) or PBS and mixed by repeated pipetting. Aliquots (250 µL) were loaded into the ultrafiltration devices and centrifuged at 2,500 rpm at 20°C for 40 min. After centrifugation, the whole device and the bottom cup with the collected filtrate were each measured in a γ-counter (PerkinElmer, Wizard^2 2480 automatic gamma counter). The retained fraction was calculated as a quotient of these measurements.

To quantify the albumin binding of the radiolabeled peptides to HSA, the radioligands (0.75 nmol or 7.5 nmol, 10-15 MBq) in a volume of 25 µL were added to 350 µL of diluted HSA/PBS solutions (containing 750 nmol to 0.075 nmol HSA; 10% or 30% commercially available HSA solution in 0.85% NaCl and 0.05% NaN_3 was used as stock solution) and mixed by repeated pipetting. Aliquots (250 µL) were loaded into the ultrafiltration devices and

centrifuged at 2,500 rpm at 20°C for 40 min. After centrifugation, 10 µL from the top and bottom fraction were measured in a γ-counter (PerkinElmer, Wizard^2 2480 automatic gamma counter). The retained fraction was calculated as a quotient of these measurements. Plots of "fraction of retained activity"=f([HSA]) were analysed using equation I (Morrison equation) to obtain K_d[HSA] values. The concentration of the radioligand was constrained to the applied value (2 or 20 µM).

n-Octanol/PBS Distribution Coefficient ($logD_{7.4}$ value).

The determination of the $logD_{7.4}$ value was done in triplicate. A sample of the ^{64}Cu-labeled compound containing ~2.5 MBq in a volume of 25 µL was added to a 2 mL Eppendorf tube containing 1.475 mL of PBS (pH 7.4) and 1.5 mL of n-octanol. The vial was vortexed vigorously for 1 min and then centrifuged at 13,500 rpm for 6 min for phase separation. The radioactivity in a defined volume of each layer was measured (ISOMED 2100). The distribution coefficient was expressed as the logarithm of the ratio of counts per minute (cpm) measured in the n-octanol phase to the cpm measured in the PBS phase.

Plasma stability assay

For human plasma, venous blood (4.5 mL) from one of two healthy, male volunteers who were not fasting or on any medication was collected. Blood samples were dispensed into S-Monovette® (Sarstedt) plasma separator tubes containing lithium heparin coated particles. The tubes were allowed to stand on ice for 30 min protected from light followed by centrifugation at 2000 rcf for 10 min at 4°C. Samples were visually checked for hemolysis and interference, stored at 4°C (protected from light) and used within a week.

For mouse plasma, arterial blood (>1 mL) from a NMRI-nu/nu mouse was obtained by heart punctuation. Blood samples were dispensed into lithium heparin (Heparin-Sodium LEO 25.000 I.U./5ml) flushed 1.5 ml Eppendorf tubes. The tubes were allowed to stand on ice for 30 min protected from light followed by centrifugation at 2000 rcf for 10 min at 4°C. Samples were visually checked for hemolysis and interference and used at the same day.

For the stability in plasma under inhibition 400 µL of plasma were incubated with 300 µM BNPP (30 mM in water) at 37°C for 1 hour. To 400 µL plasma (with or without BNPP) 10 µL of the respective radiolabeled peptide (0.465 nmol, 16.6 MBq) were added and incubated in a ThermoMixer Comfort 5355 (Eppendorf) at 37°C for up to 24 hours. At distinct time points an aliquot of 25 µL was withdrawn and diluted with a minimum of 50 µL of a mixture named "Supersol", which consists of 20% CH_3OH, 0.5% Triton X-100, 5 mM EDTA, 0.5 mM *o*-

phenanthroline and 0.1% saponin. This was followed by centrifugation at 13,500 rpm for 3 min. The supernatant was analyzed by radio HPLC.

For the determination of the identity of the metabolite formed from **NODAGA-cLAB3-TATE** in mouse plasma, **NODAGA-cLAB3-TATE** (1 µL, 2 mM, 2% DMSO) was added to a solution (1:1, v/v) of 99 µL mouse plasma in PBS (0.5 mM, pH 7.4) in a 1.5 mL Eppendorf tube. The probe was incubated for 24 h at 37°C in a thermomixer at 450 rpm. 900 µL CH_3CN:MeOH (1:1, v/v) were added and the mixture was shaken vigorously. The mixture was stored at -20°C for 1 h and was centrifugated afterwards at 15.000 g for 10 min. 100 µL of the resulting supernatant were transferred and analyzed by HPLC-HRMS as shown in Figure S8.

***In vitro* SSTR2 binding affinity**

Mouse pheochromocytoma (MPC) cells (passages 35-40) were routinely cultured in collagen-coated flasks as described elsewhere[35] and harvested at 70-80 % confluency in Dulbecco's phosphate-buffered saline containing 2.0 mM EDTA at 4 °C for 30 min. Cells were resuspended and frozen in fetal bovine serum containing 10 % (v/v) of DMSO and stored at −70 °C. After thawing, cells were washed and resuspended in ice-cold saturation assays buffer, pH 7.4, containing 50 mM Tris-HCl, 1 mM EDTA, 0.5 mM o-phenanthroline, and 0.1 % (w/v) bovine serum albumin. Cells were homogenized in ice-cold saturation assay buffer supplemented with cOmplete™ EDTA-free proteinase inhibitor (Roche, Basel Switzerland) using a Dounce homogenizer. Protein content of cell homogenates was measured at $A_{280\ nm}$ using a nanodrop spectrophotometer (Thermo-Fisher Scientific).

For measurement of total binding, 0.155 mL of cell homogenates were incubated with radioligands (A_m = 25 MBq/nmol) at increasing final concentrations between 0.625 nM and 40 nM (final sample volume 0.2 mL). For measurement of non-specific binding, specific binding sites were saturated with non-labeled DOTA-TATE at a final concentration of 1 µM. Samples were incubated for 60 min at 37°C. Incubation was stopped by soaking cell homogenates into Whatman® GF/C collection filters (GE Healthcare, Chicago, IL, USA; presoaked in 0.3 % (v/v) polyethyleneimine for 90 min) and washing with ice-cold Dulbecco's phosphate-buffered saline using a cell harvester (Brandel, Gaithersburg, MD, USA). Activity bound to filters was measured using the gamma counter Wizard (PerkinElmer). Activity in a series of radioligand standards was measured at increasing molar amounts between 0.625 – 40 nM. All measurements were performed in duplicates. Dissociation constants (K_d) and maximum binding capacities (B_{max}) were calculated as described in Figure S5 in Supporting Information.

Cell binding and internalization

MPC cells were seeded into collagen-coated 24-well microplates and cultivated for 4 days. All washing steps were performed using PBS containing 0.9 mol/L $CaCl_2$ and 0.5 mol/L $MgCl_2$. Total radioligand uptake was measured after incubation with radioligand (Am = 25 GBq/µmol) at a final concentration of 2.5 nM in RPMI 1640 medium with GlutaMAX™ supplement (Thermo Fisher Scientific) for 1 hour at 37 and 4 °C, respectively. Non-specific binding was determined in presence of non-labeled DOTA-TATE at a final concentration of 1 µM. The internalized fraction was measured after acid wash of cell surface-bound radioligand with wash buffer containing 0.05 M glycine, pH 2.8, for 5 min. Cells were lysed in 0.1 M NaOH containing 1% (w/v) sodium dodecylsulfate. Activity of cell lysates was measured using the gamma counter Wizard (PerkinElmer). Protein content of cell lysates was measured at $A_{280\ nm}$ a nanodrop spectrophotometer (Thermo-Fisher Scientific).

Experimental animals

Animal experiments were carried out according to the guidelines of the German Regulations for Animal Welfare and have been approved by the local Ethical Committee for Animal Experiments. A number of 4×10^6 MPC cells were re-suspended in 40 µL of Dulbecco's phosphate-buffered saline and injected subcutaneously into the shoulder of 7−10 week-old female nude mice (Rj:NMRI-Foxn1$^{nu/nu}$, Janvier Labs, Le Genest-Saint-Isle, France). General anesthesia was induced and maintained with inhalation of 10% (v/v) desflurane in 30/10% (v/v) oxygen/air. Tumor growth was monitored three times per week using caliper measurements. Animals were sacrificed using CO_2 inhalation and cervical dislocation.

Small animal PET/CT imaging

When diameters of MPC tumors reached 9 ± 3 mm, small-animal positron emission tomography (PET) was performed using the nanoPET/CT scanner (Mediso Medical Imaging Systems, Budapest, Hungary). Each mouse (n = 2-3) received between 7 and 10 MBq of the respective radiotracer (A_m = 40 GBq/µmoL) delivered in 0.154 M NaCl via intravenous injection through a tail vein catheter within the initial 30 s after scan start. Emission of the 511 keV annihilation photons was continuously recorded at a coincidence mode of 1-5. A series of scans were performed including four different time points after radiotracer injection, with increasing scan time, respectively (0-2 h, 5 h [4.5-5.5 h], 24 h [23-25 h], and 48 h [46-50 h]). With each PET scan, a corresponding CT image was recorded and used for anatomical referencing and attenuation correction.

Image reconstruction and data analysis

For PET image reconstruction, three-dimensional list mode data were binned using the 400-600 keV energy window. Dynamic reconstruction was performed for the initial 0-2 h scan by sorting data into 36 time frames (15×10 s, 5×30 s, 5×60 s, 4×300 s, 3×600 s, 4×900 s). Static reconstruction was performed creating one single time frame for the 5 h, 24 h, and 48 h scans, respectively. Time frames were reconstructed using the Tera-Tomo™ 3D algorithm using a voxel size of 0.4 mm and applying corrections for random events, scatter, attenuation, and decay.

Images were post-processed and analyzed using ROVER (ABX, Radeberg, Germany) and displayed as maximum intensity projection (MIPs) at indicated time points and scaling. Three-dimensional volumes of interest (VOIs) were created applying fixed thresholds for delineation of heart (frames 5-10, 50 %), kidneys (frames 10-15, 20 %), liver (frames 33-36, 30 %), muscle (frames 33-36, 0 %), tumor (frames 33-36, 30 %), and vena cava (frames 2-4, 80 %). Standardized uptake values (SUV = [MBq detected activity/mL tissue] / [MBq injected activity/g body weight], mL/g) were determined and reported as VOI-averaged SUVmean ± range. Time-activity curves were generated for all VOIs and further analyzed using Prism (GraphPad Software).

Associated Content

Supporting Information

Additional Discussions, Figures, Tables and Schemes (as mentioned in the text) and analytical data of the compounds (NMR, ESI-MS, HPLC, HRMS)

Molecular formular strings

Author Information

*E-mail: r.wodtke@hzdr.de

Conflict of interest

There are no conflicts to declare.

Acknowledgments

This research was funded by Deutsche Forschungsgemeinschaft (DFG) within the Collaborative Research Center Transregio 205/1 and 205/2 “The Adrenal: Central Relay in Health and Disease” (CRC/TRR 205/1 and 205/2; M.U. and J.P.). We cordially appreciate the expert support of Andrea Suhr for performing ^{64}Cu-labeling and the various radiometric assay methods. The authors thank Dr. Martin Kreller and the cyclotron team as well as Dr. Martin Walther and Christian Jentschel for providing [^{64}Cu]$CuCl_2$. The excellent technical assistance of Mareike Barth regarding cell culture is greatly acknowledged. The authors thank Dr. Teresia Hallström from NanoTemper Technologies for expert support and fruitful discussions concerning the MST and fluorescence-based competition assays. Furthermore, the authors wish to thank Dr. Bianca Duss and Andrea Leuschner from BAD Gesundheitsvorsorge und Sicherheitstechnik GmbH for blood draw. MPC 4/30PRR cells were kindly provided by Arthur Tischler, James Powers, and Karel Pacak.

Abbreviations used

AUC, area under curve; cLAB, “clickable” lysine-derived albumin binders; EB, Evans Blue; HSA, human serum albumin; IBU, Ibuprofen (*rac*-2-(4-Isobutylphenyl)propionic acid); MSA, murine serum albumin; MST, microscale thermophoresis; PET, positron emission tomography; PPB, plasma protein binding; SSTR2, somatostatin receptor subtype 2; SUV, standard uptake value.

References and Notes

1. Smith, D. A.; Di, L. and Kerns, E. H. The effect of plasma protein binding on in vivo efficacy: misconceptions in drug discovery. *Nat. Rev. Drug Discov.*, **2010**, *9*, 929-939.
2. Bohnert, T. and Gan, L. S. Plasma protein binding: from discovery to development. *J Pharm Sci*, **2013**, *102*, 2953-2994.
3. Liu, X.; Wright, M. and Hop, C. E. Rational use of plasma protein and tissue binding data in drug design. *J. Med. Chem.*, **2014**, *57*, 8238-8248.
4. Smith, D. A. and Rowland, M. Intracellular and intraorgan concentrations of small molecule drugs: theory, uncertainties in infectious diseases and oncology, and promise. *Drug Metab. Dispos.*, **2019**, *47*, 665-672.
5. Larsen, M. T.; Kuhlmann, M.; Hvam, M. L. and Howard, K. A. Albumin-based drug delivery: harnessing nature to cure disease. *Mol. Cell. Ther.*, **2016**, *4*, 3.
6. Zaias, J.; Mineau, M.; Cray, C.; Yoon, D. and Altman, N. H. Reference values for serum proteins of common laboratory rodent strains. *J. Am. Assoc. Lab. Anim. Sci.*, **2009**, *48*, 387-390.
7. Sand, K. M.; Bern, M.; Nilsen, J.; Noordzij, H. T.; Sandlie, I. and Andersen, J. T. Unraveling the interaction between FcRn and albumin: opportunities for design of albumin-based therapeutics. *Front. Immunol.*, **2014**, *5*, 682.
8. Bern, M.; Sand, K. M.; Nilsen, J.; Sandlie, I. and Andersen, J. T. The role of albumin receptors in regulation of albumin homeostasis: implications for drug delivery. *J. Control. Release*, **2015**, *211*, 144-162.
9. Knudsen, L. B. and Lau, J. The discovery and development of liraglutide and semaglutide. *Front. Endocrinol.*, **2019**, *10*, 155.

10. Jonassen, I.; Havelund, S.; Hoeg-Jensen, T.; Steensgaard, D. B.; Wahlund, P. O. and Ribel, U. Design of the novel protraction mechanism of insulin degludec, an ultra-long-acting basal insulin. *Pharm. Res.*, **2012**, *29*, 2104-2114.
11. Home, P. and Kurtzhals, P. Insulin detemir: from concept to clinical experience. *Expert Opin. Pharmacother.*, **2006**, *7*, 325-343.
12. Donner, T. and Sarkar, S., Pharmacology, therapeutic regimens, and principles of intensive insulin therapy. [Updated 2019 Feb 23]. In *Endotext [Internet]*. Eds. K. R. Feingold, B. Anawalt, A. Boyce, G. Chrousos, W. W. de Herder, K. Dhatariya, K. Dungan, J. M. Hershman, J. Hofland, S. Kalra, G. Kaltsas, C. Koch, P. Kopp, M. Korbonits, C. S. Kovacs, W. Kuohung, B. Laferrère, M. Levy, E. A. McGee, R. McLachlan, J. E. Morley, M. New, J. Purnell, R. Sahay, F. Singer, M. A. Sperling, C. A. Stratakis, D. L. Trence and D. P. Wilson, MDText.com, Inc., South Dartmouth (MA), 2000, https://www.ncbi.nlm.nih.gov/books/NBK278938/?report=classic.
13. Hoogenboezem, E. N. and Duvall, C. L. Harnessing albumin as a carrier for cancer therapies. *Adv. Drug Deliv. Rev.*, **2018**, *130*, 73-89.
14. Villaverde, G. and Baeza, A. Targeting strategies for improving the efficacy of nanomedicine in oncology. *Beilstein J. Nanotechnol.*, **2019**, *10*, 168-181.
15. Rahimizadeh, P.; Yang, S. and Lim, S. I. Albumin: an emerging opportunity in drug delivery. *Biotechnol. Bioprocess Eng.*, **2020**, *25*, 985-995.
16. Brandt, M.; Cardinale, J.; Giammei, C.; Guarrochena, X.; Happl, B.; Jouini, N. and Mindt, T. L. Mini-review: targeted radiopharmaceuticals incorporating reversible, low molecular weight albumin binders. *Nucl. Med. Biol.*, **2019**, *70*, 46-52.
17. Minczeles, N. S.; Hofland, J.; de Herder, W. W. and Brabander, T. Strategies towards improving clinical outcomes of peptide receptor radionuclide therapy. *Curr. Oncol. Rep.*, **2021**, *23*, 46.
18. Müller, C.; Struthers, H.; Winiger, C.; Zhernosekov, K. and Schibli, R. DOTA conjugate with an albumin-binding entity enables the first folic acid-targeted ^{177}Lu-radionuclide tumor therapy in mice. *J. Nucl. Med.*, **2013**, *54*, 124-131.
19. Tian, R.; Jacobson, O.; Niu, G.; Kiesewetter, D. O.; Wang, Z.; Zhu, G.; Ma, Y.; Liu, G. and Chen, X. Evans blue attachment enhances somatostatin receptor subtype-2 imaging and radiotherapy. *Theranostics*, **2018**, *8*, 735-745.
20. Kelly, J. M.; Amor-Coarasa, A.; Nikolopoulou, A.; Wustemann, T.; Barelli, P.; Kim, D.; Williams, C., Jr.; Zheng, X.; Bi, C.; Hu, B.; Warren, J. D.; Hage, D. S.; DiMagno, S. G. and Babich, J. W. Dual-target binding ligands with modulated pharmacokinetics for endoradiotherapy of prostate cancer. *J. Nucl. Med.*, **2017**, *58*, 1442-1449.
21. Höltke, C.; Alsibai, W.; Grewer, M.; Stolting, M.; Geyer, C.; Eisenblatter, M.; Wildgruber, M. and Helfen, A. How different albumin-binders drive probe distribution of fluorescent RGD mimetics. *Front. Chem.*, **2021**, *9*.
22. Höltke, C.; Grewer, M.; Stolting, M.; Geyer, C.; Wildgruber, M. and Helfen, A. Exploring the influence of different albumin binders on molecular imaging probe distribution. *Mol. Pharm.*, **2021**, *18*, 2574-2585.
23. Garnier, L.; Gkountidi, A. O. and Hugues, S. Tumor-associated lymphatic vessel features and immunomodulatory functions. *Front. Immunol.*, **2019**, *10*, 720.
24. Golombek, S. K.; May, J. N.; Theek, B.; Appold, L.; Drude, N.; Kiessling, F. and Lammers, T. Tumor targeting via EPR: strategies to enhance patient responses. *Adv. Drug Deliv. Rev.*, **2018**, *130*, 17-38.
25. Bertrand, N.; Wu, J.; Xu, X.; Kamaly, N. and Farokhzad, O. C. Cancer nanotechnology: the impact of passive and active targeting in the era of modern cancer biology. *Adv. Drug Deliv. Rev.*, **2014**, *66*, 2-25.
26. Mier, W.; Babich, J. and Haberkorn, U. Is nano too big? *Eur. J. Nucl. Med. Mol. Imaging*, **2014**, *41*, 4-6.
27. Song, S.; Zhang, Y.; Ding, T.; Ji, N. and Zhao, H. The dual role of macropinocytosis in cancers: promoting growth and inducing methuosis to participate in anticancer therapies as targets. *Front. Oncol.*, **2020**, *10*, 570108.
28. Merlot, A. M.; Kalinowski, D. S. and Richardson, D. R. Unraveling the mysteries of serum albumin-more than just a serum protein. *Front. Physiol.*, **2014**, *5*, 299.
29. Park, C. R.; Jo, J. H.; Song, M. G.; Park, J. Y.; Kim, Y. H.; Youn, H.; Paek, S. H.; Chung, J. K.; Jeong, J. M.; Lee, Y. S. and Kang, K. W. Secreted protein acidic and rich in cysteine mediates active targeting of human serum albumin in U87MG xenograft mouse models. *Theranostics*, **2019**, *9*, 7447-7457.
30. Davidson, S. M.; Jonas, O.; Keibler, M. A.; Hou, H. W.; Luengo, A.; Mayers, J. R.; Wyckoff, J.; Del Rosario, A. M.; Whitman, M.; Chin, C. R.; Condon, K. J.; Lammers, A.; Kellersberger, K. A.; Stall, B. K.; Stephanopoulos, G.; Bar-Sagi, D.; Han, J.; Rabinowitz, J. D.; Cima, M. J.; Langer, R. and Vander Heiden, M. G. Direct evidence for cancer-cell-autonomous extracellular protein catabolism in pancreatic tumors. *Nat. Med.*, **2017**, *23*, 235-241.
31. Dumelin, C. E.; Trussel, S.; Buller, F.; Trachsel, E.; Bootz, F.; Zhang, Y.; Mannocci, L.; Beck, S. C.; Drumea-Mirancea, M.; Seeliger, M. W.; Baltes, C.; Muggler, T.; Kranz, F.; Rudin, M.; Melkko, S.; Scheuermann, J. and Neri, D. A portable albumin binder from a DNA-encoded chemical library. *Angew. Chem. Int. Ed. Engl.*, **2008**, *47*, 3196-3201.
32. Mindt, T. L.; Struthers, H.; Spingler, B.; Brans, L.; Tourwe, D.; Garcia-Garayoa, E. and Schibli, R. Molecular assembly of multifunctional ^{99m}Tc radiopharmaceuticals using "clickable" amino acid derivatives. *ChemMedChem*, **2010**, *5*, 2026-2038.

33. Xu, C. and Zhang, H. Somatostatin receptor based imaging and radionuclide therapy. *Biomed. Res. Int.*, **2015**, *2015*, 917968.
34. Hennrich, U. and Kopka, K. Lutathera®: the first FDA- and EMA-approved radiopharmaceutical for peptide receptor radionuclide therapy. *Pharmaceuticals*, **2019**, *12*.
35. Ullrich, M.; Bergmann, R.; Peitzsch, M.; Cartellieri, M.; Qin, N.; Ehrhart-Bornstein, M.; Block, N. L.; Schally, A. V.; Pietzsch, J.; Eisenhofer, G.; Bornstein, S. R. and Ziegler, C. G. In vivo fluorescence imaging and urinary monoamines as surrogate biomarkers of disease progression in a mouse model of pheochromocytoma. *Endocrinology*, **2014**, *155*, 4149-4156.
36. Ullrich, M.; Bergmann, R.; Peitzsch, M.; Zenker, E. F.; Cartellieri, M.; Bachmann, M.; Ehrhart-Bornstein, M.; Block, N. L.; Schally, A. V.; Eisenhofer, G.; Bornstein, S. R.; Pietzsch, J. and Ziegler, C. G. Multimodal somatostatin receptor theranostics using [^{64}Cu]Cu-/[^{177}Lu]Lu-DOTA-(Tyr^{3})octreotate and AN-238 in a mouse pheochromocytoma model. *Theranostics*, **2016**, *6*, 650-665.
37. Seifert, V.; Richter, S.; Bechmann, N.; Bachmann, M.; Ziegler, C. G.; Pietzsch, J. and Ullrich, M. HIF2alpha-associated pseudohypoxia promotes radioresistance in pheochromocytoma: Insights from 3D models. *Cancers*, **2021**, *13*, 385.
38. Ullrich, M.; Liers, J.; Peitzsch, M.; Feldmann, A.; Bergmann, R.; Sommer, U.; Richter, S.; Bornstein, S. R.; Bachmann, M.; Eisenhofer, G.; Ziegler, C. G. and Pietzsch, J. Strain-specific metastatic phenotypes in pheochromocytoma allograft mice. *Endocr. Relat. Cancer*, **2018**, *25*, 993-1004.
39. Bechmann, N.; Poser, I.; Seifert, V.; Greunke, C.; Ullrich, M.; Qin, N.; Walch, A.; Peitzsch, M.; Robledo, M.; Pacak, K.; Pietzsch, J.; Richter, S. and Eisenhofer, G. Impact of extrinsic and intrinsic hypoxia on catecholamine biosynthesis in absence or presence of Hif2alpha in pheochromocytoma cells. *Cancers*, **2019**, *11*, 594.
40. Nolting, S.; Ullrich, M.; Pietzsch, J.; Ziegler, C. G.; Eisenhofer, G.; Grossman, A. and Pacak, K. Current management of pheochromocytoma/paraganglioma: A guide for the practicing clinician in the era of precision medicine. *Cancers*, **2019**, *11*.
41. Jerabek-Willemsen, M.; André, T.; Wanner, R.; Roth, H. M.; Duhr, S.; Baaske, P. and Breitsprecher, D. Microscale thermophoresis: Interaction analysis and beyond. *J . Mol. Struc.*, **2014**, *1077*, 101-113.
42. Seidel, S. A.; Dijkman, P. M.; Lea, W. A.; van den Bogaart, G.; Jerabek-Willemsen, M.; Lazic, A.; Joseph, J. S.; Srinivasan, P.; Baaske, P.; Simeonov, A.; Katritch, I.; Melo, F. A.; Ladbury, J. E.; Schreiber, G.; Watts, A.; Braun, D. and Duhr, S. Microscale thermophoresis quantifies biomolecular interactions under previously challenging conditions. *Methods*, **2013**, *59*, 301-315.
43. Pant, K.; Pufe, J.; Zarschler, K.; Bergmann, R.; Steinbach, J.; Reimann, S.; Haag, R.; Pietzsch, J. and Stephan, H. Surface charge and particle size determine the metabolic fate of dendritic polyglycerols. *Nanoscale*, **2017**, *9*, 8723-8739.
44. Müller, C.; Farkas, R.; Borgna, F.; Schmid, R. M.; Benesova, M. and Schibli, R. Synthesis, radiolabeling, and characterization of plasma protein-binding ligands: Potential tools for modulation of the pharmacokinetic properties of (radio)pharmaceuticals. *Bioconjug. Chem.*, **2017**, *28*, 2372-2383.
45. Ghuman, J.; Zunszain, P. A.; Petitpas, I.; Bhattacharya, A. A.; Otagiri, M. and Curry, S. Structural basis of the drug-binding specificity of human serum albumin. *J. Mol. Biol.*, **2005**, *353*, 38-52.
46. Czub, M. P.; Handing, K. B.; Venkataramany, B. S.; Cooper, D. R.; Shabalin, I. G. and Minor, W. Albumin-based transport of nonsteroidal anti-inflammatory drugs in mammalian blood plasma. *J. Med. Chem.*, **2020**, *63*, 6847-6862.
47. Zielinski, K.; Sekula, B.; Bujacz, A. and Szymczak, I. Structural investigations of stereoselective profen binding by equine and leporine serum albumins. *Chirality*, **2020**, *32*, 334-344.
48. Tso, S. C.; Chen, Q.; Vishnivetskiy, S. A.; Gurevich, V. V.; Iverson, T. M. and Brautigam, C. A. Using two-site binding models to analyze microscale thermophoresis data. *Anal. Biochem.*, **2018**, *540-541*, 64-75.
49. Scheuermann, T. H.; Padrick, S. B.; Gardner, K. H. and Brautigam, C. A. On the acquisition and analysis of microscale thermophoresis data. *Anal. Biochem.*, **2016**, *496*, 79-93.
50. Klymchenko, A. S. Solvatochromic and fluorogenic dyes as environment-sensitive probes: design and biological applications. *Acc. Chem. Res.*, **2017**, *50*, 366-375.
51. Sjöback, R.; Nygren, J. and Kubista, M. Absorption and fluorescence properties of fluorescein. *Spectrochim. Acta A Mol. Biomol. Spectrosc.*, **1995**, *51*, L7-L21.
52. Lorand, L.; Lockridge, O. M.; Campbell, L. K.; Myhrman, R. and Bruner-Lorand, J. Transamidating enzymes. II. A continuous fluorescent method suited for automating measurements of factor XIII in plasma. *Anal. Biochem.*, **1971**, *44*, 221-231.
53. Case, A. and Stein, R. L. Kinetic analysis of the action of tissue transglutaminase on peptide and protein substrates. *Biochemistry*, **2003**, *42*, 9466-9481.
54. Brautigam, C. A. Calculations and publication-quality illustrations for analytical ultracentrifugation data. *Methods Enzymol.*, **2015**, *562*, 109-133.
55. Recnik, L. M.; Kandioller, W. and Mindt, T. L. 1,4-Disubstituted 1,2,3-triazoles as amide bond surrogates for the stabilisation of linear peptides with biological activity. *Molecules*, **2020**, *25*.
56. Deberle, L. M.; Benesova, M.; Umbricht, C. A.; Borgna, F.; Buchler, M.; Zhernosekov, K.; Schibli, R. and Müller, C. Development of a new class of PSMA radioligands comprising ibuprofen as an albumin-binding entity. *Theranostics*, **2020**, *10*, 1678-1693.

57. Charton, M. Steric effects. I. esterification and acid-catalyzed hydrolysis of esters. *J. Am. Chem. Soc.*, **1975**, *97*, 1552-1555.
58. Hansch, C. and Leo, A., *Exploring QSAR Fundamentals and Applications in Chemistry and Biology*, American Chemical Society, USA, 1995.
59. Hansch, C.; Leo, A. and Hoekman, D., *Exploring QSAR: Hydrophobic, Electronic, and Steric Constants*, American Chemical Society, USA, 1995.
60. Druckrey, E. Regressionsanalyse von Struktur-Wirkungs-Beziehungen (Hansch-Analyse). *Pharm. unserer Zeit*, **1975**, *4*, 145-150.
61. Kubinyi, H., *QSAR: Hansch Analysis and Related Approaches*, VCH, Weinheim, 1993.
62. Rousseau, E.; Lau, J.; Zhang, Z.; Uribe, C. F.; Kuo, H. T.; Zhang, C.; Zeisler, J.; Colpo, N.; Lin, K. S. and Benard, F. Effects of adding an albumin binder chain on [^{177}Lu]Lu-DOTATATE. *Nucl. Med. Biol.*, **2018**, *66*, 10-17.
63. Jong, M. d.; Breeman, W.; Bakker, W.; Kooij, P.; Bernard, B.; Hofland, L.; Visser, T.; Srinivasan, A.; Schmidt, M.; Erion, J.; Bugaj, J.; Mäcke, H. and Krenning, E. Comparison of ^{111}In-labeled somatostatin analogues for tumor scintigraphy and radionuclide therapy. *Cancer Res.*, **1998**, *58 3*, 437-441.
64. Reubi, J. C.; Schar, J. C.; Waser, B.; Wenger, S.; Heppeler, A.; Schmitt, J. S. and Macke, H. R. Affinity profiles for human somatostatin receptor subtypes SST1-SST5 of somatostatin radiotracers selected for scintigraphic and radiotherapeutic use. *Eur. J. Nucl. Med.*, **2000**, *27*, 273-282.
65. Tam, J. P.; Wu, C. R.; Liu, W. and Zhang, J. W. Disulfide bond formation in peptides by dimethyl-sulfoxide - scope and applications. *J. Am. Chem. Soc.*, **1991**, *113*, 6657-6662.
66. Hsieh, H. P.; Wu, Y. T.; Chen, S. T. and Wang, K. T. Direct solid-phase synthesis of octreotide conjugates: precursors for use as tumor-targeted radiopharmaceuticals. *Bioorg. Med. Chem.*, **1999**, *7*, 1797-1803.
67. FDA drug label, https://www.accessdata.fda.gov/drugsatfda_docs/nda/2018/208700Orig1s000lbll.pdf, (accessed 12/10/21).
68. Advanced Accelerator Applications, Product Monograph LUTATHERA®, https://www.samnordic.se/wp-content/uploads/2018/05/LUTATHERA-MONOGRAPH-120218.pdf, (accessed 12/10/21).
69. Laznicek, M.; Laznickova, A.; Mäcke, H. R.; Eisenwiener, K.; Reubi, J. C. and Wenger, S. Octreotide and octreotate derivatives radiolabeled with yttrium: pharmacokinetics in rats. *Cancer Biother. Radiopharm.*, **2002**, *17*, 527-533.
70. Jarmoskaite, I.; AlSadhan, I.; Vaidyanathan, P. P. and Herschlag, D. How to measure and evaluate binding affinities. *eLife*, **2020**, *9*.
71. Zhang, B.; Wang, Y.; Gao, M.; Gu, M. and Wang, C. Tris(hydroxymethyl)aminomethane-functionalized agarose particles: parameters affecting the binding of bovine serum albumin. *J. Sep. Sci.*, **2012**, *35*, 1406-1410.
72. Sokolowska, M.; Pawlas, K. and Bal, W. Effect of common buffers and heterocyclic ligands on the binding of Cu(II) at the multimetal binding site in human serum albumin. *Bioinorg. Chem. Appl.*, **2010**, DOI: 10.1155/2010/725153, 725153.
73. Hulme, E. C. and Trevethick, M. A. Ligand binding assays at equilibrium: validation and interpretation. *Br. J. Pharmacol.*, **2010**, *161*, 1219-1237.
74. Hochscherf, J.; Lindenblatt, D.; Steinkruger, M.; Yoo, E.; Ulucan, O.; Herzig, S.; Issinger, O. G.; Helms, V.; Gotz, C.; Neundorf, I.; Niefind, K. and Pietsch, M. Development of a high-throughput screening-compatible assay to identify inhibitors of the CK2α/CK2β interaction. *Anal. Biochem.*, **2015**, *468*, 4-14.
75. Qi, J.; Kizjakina, K.; Robinson, R.; Tolani, K. and Sobrado, P. A fluorescence polarization binding assay to identify inhibitors of flavin-dependent monooxygenases. *Anal. Biochem.*, **2012**, *425*, 80-87.
76. Schottelius, M.; Simecek, J.; Hoffmann, F.; Willibald, M.; Schwaiger, M. and Wester, H. J. Twins in spirit - episode I: comparative preclinical evaluation of [^{68}Ga]DOTATATE and [^{68}Ga]HA-DOTATATE. *EJNMMI Res.*, **2015**, *5*, 22.
77. Siwowska, K.; Haller, S.; Bortoli, F.; Benesova, M.; Groehn, V.; Bernhardt, P.; Schibli, R. and Müller, C. Preclinical comparison of albumin-binding radiofolates: impact of linker entities on the in vitro and in vivo properties. *Mol. Pharm.*, **2017**, *14*, 523-532.
78. Benesova, M.; Umbricht, C. A.; Schibli, R. and Müller, C. Albumin-binding PSMA ligands: optimization of the tissue distribution profile. *Mol. Pharm.*, **2018**, *15*, 934-946.
79. Powers, J. F.; Evinger, M. J.; Tsokas, P.; Bedri, S.; Alroy, J.; Shahsavari, M. and Tischler, A. S. Pheochromocytoma cell lines from heterozygous neurofibromatosis knockout mice. *Cell Tissue Res.*, **2000**, *302*, 309-320.
80. Tummino, P. J. and Copeland, R. A. Residence time of receptor-ligand complexes and its effect on biological function. *Biochemistry*, **2008**, *47*, 5481-5492.
81. Crozat, A.; Penhoat, A. and Saez, J. M. Processing of angiotensin II (A-II) and (Sar^{1},Ala^{8})A-II by cultured bovine adrenocortical cells. *Endocrinology*, **1986**, *118*, 2312-2318.
82. Li, B.; Sedlacek, M.; Manoharan, I.; Boopathy, R.; Duysen, E. G.; Masson, P. and Lockridge, O. Butyrylcholinesterase, paraoxonase, and albumin esterase, but not carboxylesterase, are present in human plasma. *Biochem. Pharmacol.*, **2005**, *70*, 1673-1684.
83. Wang, D.; Zou, L.; Jin, Q.; Hou, J.; Ge, G. and Yang, L. Human carboxylesterases: a comprehensive review. *Acta Pharm. Sin. B*, **2018**, *8*, 699-712.

84. Lv, X.; Wang, D.-D.; Feng, L.; Wang, P.; Zou, L.-W.; Hao, D.-C.; Hou, J.; Cui, J.-N.; Ge, G.-B. and Yang, L. A highly selective marker reaction for measuring the activity of human carboxylesterase 1 in complex biological samples. *RSC Advances*, **2016**, *6*, 4302-4309.
85. Di, L. The impact of carboxylesterases in drug metabolism and pharmacokinetics. *Curr. Drug Metab.*, **2019**, *20*, 91-102.
86. Berry, L. M.; Wollenberg, L. and Zhao, Z. Esterase activities in the blood, liver and intestine of several preclinical species and humans. *Drug Metab. Lett.*, **2009**, *3*, 70-77.
87. Heymann, E. and Krisch, K. Phosphorsäure-bis-(*p*-nitro-phenylester), ein neuer Hemmstoff mikrosomaler Carboxylesterasen. *Hoppe Seylers Z Physiol. Chem.*, **1967**, *348*, 609-619.
88. Eng, H.; Niosi, M.; McDonald, T. S.; Wolford, A.; Chen, Y.; Simila, S. T.; Bauman, J. N.; Warmus, J. and Kalgutkar, A. S. Utility of the carboxylesterase inhibitor bis-para-nitrophenylphosphate (BNPP) in the plasma unbound fraction determination for a hydrolytically unstable amide derivative and agonist of the TGR5 receptor. *Xenobiotica*, **2010**, *40*, 369-380.
89. Dumont, R. A.; Deininger, F.; Haubner, R.; Maecke, H. R.; Weber, W. A. and Fani, M. Novel ^{64}Cu- and ^{68}Ga-labeled RGD conjugates show improved PET imaging of $\alpha_v\beta_3$ integrin expression and facile radiosynthesis. *J. Nucl. Med.*, **2011**, *52*, 1276-1284.
90. Wadas, T. J.; Wong, E. H.; Weisman, G. R. and Anderson, C. J. Copper chelation chemistry and its role in copper radiopharmaceuticals. *Curr. Pharm. Des.*, **2007**, *13*, 3-16.
91. Gupta, A. and Lutsenko, S. Human copper transporters: mechanism, role in human diseases and therapeutic potential. *Future Med. Chem.*, **2009**, *1*, 1125-1142.
92. Qin, C.; Liu, H.; Chen, K.; Hu, X.; Ma, X.; Lan, X.; Zhang, Y. and Cheng, Z. Theranostics of malignant melanoma with $^{64}CuCl_2$. *J. Nucl. Med.*, **2014**, *55*, 812-817.
93. Garcia-Perez, F. O.; Medina-Ornelas, S. S.; Barron-Barron, F. and Arrieta-Rodriguez, O. Evaluation of non-small cell lung cancer by PET/CT with $^{64}CuCl_2$: initial experience in humans. *Am. J. Nucl. Med. Mol. Imaging*, **2020**, *10*, 143-150.
94. Blakeley, D.; Sykes, D. A.; Ensor, P.; Bertran, E.; Aston, P. J. and Charlton, S. J. Simulating the influence of plasma protein on measured receptor affinity in biochemical assays reveals the utility of Schild analysis for estimating compound affinity for plasma proteins. *Br. J. Pharmacol.*, **2015**, *172*, 5037-5049.
95. Kawai, K.; Nishii, R.; Shikano, N.; Makino, N.; Kuga, N.; Yoshimoto, M.; Jinnouchi, S.; Nagamachi, S.; Tamura, S. and Takamura, N. Serum protein binding displacement: theoretical analysis using a hypothetical radiopharmaceutical and experimental analysis with ^{123}I-N-isopropyl-*p*-iodoamphetamine. *Nucl. Med. Biol.*, **2009**, *36*, 99-106.
96. Umbricht, C. A.; Benesova, M.; Schibli, R. and Müller, C. Preclinical development of novel PSMA-targeting radioligands: modulation of albumin-binding properties to improve prostate cancer therapy. *Mol. Pharm.*, **2018**, *15*, 2297-2306.
97. Heneweer, C.; Holland, J. P.; Divilov, V.; Carlin, S. and Lewis, J. S. Magnitude of enhanced permeability and retention effect in tumors with different phenotypes: ^{89}Zr-albumin as a model system. *J. Nucl. Med.*, **2011**, *52*, 625-633.
98. Kalliokoski, A. and Niemi, M. Impact of OATP transporters on pharmacokinetics. *Br. J. Pharmacol.*, **2009**, *158*, 693-705.
99. Varma, M. V.; El-Kattan, A. F.; Feng, B.; Steyn, S. J.; Maurer, T. S.; Scott, D. O.; Rodrigues, A. D. and Tremaine, L. M. Extended clearance classification system (ECCS) informed approach for evaluating investigational drugs as substrates of drug transporters. *Clin. Pharmacol. Ther.*, **2017**, *102*, 33-36.
100. Chen, H.; Jacobson, O.; Niu, G.; Weiss, I. D.; Kiesewetter, D. O.; Liu, Y.; Ma, Y.; Wu, H. and Chen, X. Novel "add-on" molecule based on evans blue confers superior pharmacokinetics and transforms drugs to theranostic agents. *J. Nucl. Med.*, **2017**, *58*, 590-597.
101. Tiel, S. v.; Maina, T.; Nock, B.; Konijnenberg, M.; Blois, E. d.; Seimbille, Y.; Bernsen, M. and Jong, M. d. Albutate-1, a novel long-circulating radiotracer targeting the somatostatin receptor subtype 2. *JNMRS*, **2021**, DOI: 10.31487/j.JNMRS.2021.01.01, 1-9.
102. Bandara, N.; Jacobson, O.; Mpoy, C.; Chen, X. and Rogers, B. E. Novel structural modification based on evans blue dye to improve pharmacokinetics of a somastostatin-receptor-based theranostic agent. *Bioconjug. Chem.*, **2018**, *29*, 2448-2454.
103. Hanscheid, H.; Hartrampf, P. E.; Schirbel, A.; Buck, A. K. and Lapa, C. Intraindividual comparison of [^{177}Lu]Lu-DOTA-EB-TATE and [^{177}Lu]Lu-DOTA-TOC. *Eur. J. Nucl. Med. Mol. Imaging*, **2021**, *48*, 2566-2572.
104. Zhang, J.; Wang, H.; Jacobson, O.; Cheng, Y.; Niu, G.; Li, F.; Bai, C.; Zhu, Z. and Chen, X. Safety, pharmacokinetics, and dosimetry of a long-acting radiolabeled somatostatin analog ^{177}Lu-DOTA-EB-TATE in patients with advanced metastatic neuroendocrine tumors. *J. Nucl. Med.*, **2018**, *59*, 1699-1705.
105. Gassner, C.; Neuber, C.; Laube, M.; Bergmann, R.; Kniess, T. and Pietzsch, J. Development of a ^{18}F-labeled diaryl-substituted dihydropyrrolo[3,2,1-*hi*]indole as potential probe for functional imaging of cyclooxygenase-2 with PET. *ChemistrySelect*, **2016**, *1*, 5812-5820.
106. Wodtke, R.; Wodtke, J.; Hauser, S.; Laube, M.; Bauer, D.; Rothe, R.; Neuber, C.; Pietsch, M.; Kopka, K.; Pietzsch, J. and Löser, R. Development of an ^{18}F-labeled irreversible inhibitor of transglutaminase 2 as radiometric tool for quantitative expression profiling in cells and tissues. *J. Med. Chem.*, **2021**, *64*, 3462-3478.

107. Donovan, S. F. and Pescatore, M. C. Method for measuring the logarithm of the octanol–water partition coefficient by using short octadecyl–poly(vinyl alcohol) high-performance liquid chromatography columns. *J. Chromatogr. A*, **2002**, *952*, 47-61.
108. Valko, K.; Nunhuck, S.; Bevan, C.; Abraham, M. H. and Reynolds, D. P. Fast gradient HPLC method to determine compounds binding to human serum albumin. Relationships with octanol/water and immobilized artificial membrane lipophilicity. *J. Pharm. Sci.*, **2003**, *92*, 2236-2248.
109. Kreller, M.; Pietzsch, H.; Walther, M.; Tietze, H.; Kaever, P.; Knieß, T.; Füchtner, F.; Steinbach, J. and Preusche, S. Introduction of the new center for radiopharmaceutical cancer research at Helmholtz-Zentrum Dresden-Rossendorf. *Instruments*, **2019**, *3*, 9.
110. Thieme, S.; Walther, M.; Pietzsch, H. J.; Henniger, J.; Preusche, S.; Mading, P. and Steinbach, J. Module-assisted preparation of ^{64}Cu with high specific activity. *Appl. Radiat. Isot.*, **2012**, *70*, 602-608.

Table of Contents Graphic

Modifying the kinetic profile of tumour uptake by albumin binders